Leveraging Generative Artificial Intelligence for Uplink Feedback-Free Transmission in 6G FD-RAN

Haibo Zhou, *Fellow, IEEE*, Yunting Xu, *Member, IEEE*, Tianqi Zhang, *Member, IEEE*, Xin Zhang, *Member, IEEE*, Jiacheng Chen, *Member, IEEE*, and Xuemin Shen, *Fellow, IEEE*

***Abstract*—Cooperative uplink multi-base station (BS) reception has emerged as a promising technology to enhance received signal strength and improve wireless spectral efficiency. However, realizing the potential performance gains remains challenging due to substantial communication overhead among cooperative BSs and excessive delays in channel state information (CSI) feedback. This paper investigates a CSI feedback-free mechanism that leverages time-invariant physical layer parameters to facilitate cooperative BS reception within a fully-decoupled radio access network (FD-RAN). First, given the dynamically changing characteristics of the wireless environment, we employ conditional variational autoencoder (CVAE), a state-of-the-art generative artificial intelligence (GAI) approach, to generate location-specific representative channels for calculating CSI feedback-free transmission parameters. Subsequently, to maximize the throughput of user equipment (UE), a diffusion model-based deep reinforcement learning (DRL) framework is proposed for jointly selecting cooperative BS reception sets and precoding schemes, utilizing the representative channels generated by CVAE. Extensive simulations conducted on a link-level simulator demonstrate that the proposed CSI feedback-free mechanism for cooperative multi-BS reception can effectively improve spectrum efficiency by 17.3%, which provides a promising design principle for the development of sixth-generation (6G) wireless networks.**

***Index Terms*—Cooperative BS reception, feedback-free transmission, FD-RAN, variational encoder, generative AI.**

I. Introduction

With the growing demands for enhanced spectral efficiency and network capacity in wireless access systems, cooperative multi-base station (BS) reception is increasingly regarded as a pivotal technology to facilitate user-centric services for next-generation wireless networks [1], [2], [3]. Compared to traditional point-to-point cellular systems in Long Term Evolution (LTE) and fifth-generation (5G) mobile networks, cooperative multi-BS reception transforms interference signals from neighboring cells into useful signals, demonstrating significant enhancement in the received signal strength without increasing the total transmit power [4]. However, the performance gains achieved through multi-BS reception necessitate frequent exchanges of real-time channel state information (CSI) among cooperative BSs, thus resulting in substantial communication overhead [5]. Additionally, due to the variation in wireless conditions across different BSs, the instantaneous CSI measured by the BSs with large feedback delay would become outdated, failing to accurately reflect the real-time channel status and significantly impairing the overall performance of multi-BS reception [6]. Furthermore, when determining the cooperative BS reception set for each user equipment (UE), the computation complexity increases exponentially with the number of participating BSs, making it computationally prohibitive to dynamically reconfigure BS reception set based on real-time channel status [7].

To alleviate the communication and computational overhead of cooperative multi-BS reception, long-term channel statistics, such as covariance matrix [8] and large-scale fading (LSF) coefficient [9], have been extensively exploited to derive the ergodic rate expressions and calculate the cooperative BS set. Although these statistical CSI-based schemes can theoretically obtain the capacity upper bounds of multi-BS reception, they fail to capture essential real-time link adaptation metrics such as the precoding matrix indicator (PMI), rank indicator (RI), and channel quality indicator (CQI) for practical physical layer transmission [10]. Moreover, as LSF conditions evolve over time, the cooperative BS set needs to be frequently recomputed, leading to substantial overhead and limited scalability. Recently, a CSI feedback-free transmission mechanism, introduced by the fully-decoupled radio access network (FD-RAN) [11], [12], [13], has emerged as a promising solution for efficient and flexible multi-BS coordination. Different from traditional CSI feedback mechanisms or methods relying on statistical channel information, the FD-RAN employs fixed PMI, RI, CQI, and cooperative BS set predetermined from the UE's geographic position. This feedback-free design effectively mitigates the computational burden associated with real-time CSI processing, and overcomes the inherent limitation of statistical CSI in link adaptation parameter design [14], [15].

However, despite the adoption of fixed physical layer transmission parameters in the feedback-free FD-RAN mechanism

Received 21 August 2025; revised 6 November 2025; accepted 1 December 2025. Date of publication 8 December 2025; date of current version 6 April 2026. This work was supported by the National Natural Science Foundation of China under Grant 62271244. Recommended for acceptance by X. Yu. *(Corresponding author: Yunting Xu.)*

Haibo Zhou, Tianqi Zhang, and Xin Zhang are with the School of Electronic Science and Engineering, Nanjing University, Nanjing 210023, China (e-mail: haibozhou@nju.edu.cn; tianqizhang@smail.nju.edu.cn; xinzhang@nju.edu.cn).

Yunting Xu is with the College of Computing and Data Science, Nanyang Technological University, Singapore 639798 (e-mail: yunting.xu@ntu.edu.sg).

Jiacheng Chen is with the Department of Strategic and Advanced Interdisciplinary Research, Peng Cheng Laboratory, Shenzhen 518000, China (e-mail: chenjch02@pcl.ac.cn).

Xuemin Shen is with the Department of Electrical and Computer Engineering, University of Waterloo, Waterloo, ON N2L 3G1, Canada (e-mail: sshen@uwaterloo.ca).

Digital Object Identifier 10.1109/TMC.2025.3640955

to substantially reduce cooperative overhead for uplink multi-BS reception, the determination of static transmission parameters remains challenging due to the dynamically changing wireless environment [16], [17]. In particular, under rapidly varying channel conditions with significant stochastic fluctuations across different time subframes, inappropriate physical layer parameters may lead to an elevated transmission bit error rate (BER) [18]. Recent revolutionary advances in generative artificial intelligence (GenAI), such as generative adversarial networks (GANs), variational autoencoders (VAEs), and diffusion models, have demonstrated remarkable capabilities in characterizing dynamic environmental features [19], [20], [21]. By fitting the distribution of historical channel data, GenAI models are capable of generating a time-domain representative channel [22], which can be utilized for the calculation of fixed physical layer transmission parameters and cooperative BS sets. Compared to traditional statistical model-based methods, representative channels generated through GenAI models offer improved adaptability to dynamic channel characteristics across different subframes, thereby providing an effective solution for computing CSI feedback-free transmission schemes in FD-RAN and enhancing the overall performance of feedback-free multi-BS transmissions [23], [24], [25].

Motivated by the feedback-free FD-RAN architecture and the superior generation capability of GenAI model, this paper aims to design a scalable uplink multi-BS reception scheme that maximizes UE throughput while reducing the communication and computational overhead induced by real-time CSI feedback. Specifically, we employ GenAI to capture the underlying channel distribution based on historical channel data collected from multiple transmission subframes. The well-trained GenAI model then synthesizes location-specific representative channels that closely match the statistical characteristics of the historical CSI data. Based on these representative channels, fixed physical-layer parameters, including PMI, RI, CQI, and cooperative BS selection, are computed offline to predefine the precoding matrix, number of MIMO streams, modulation and coding scheme (MCS), and BS set within the FD-RAN architecture. These parameters are consistently applied across all transmission periods, thereby eliminating the substantial overhead associated with real-time CSI feedback. The main contributions of this paper are summarized as follows:

- We propose a conditional VAE (CVAE)-based GenAI model to synthesize location-specific representative channels that match the distribution of historical channel data. These synthesized channels are utilized to compute CSI feedback-free transmission schemes for cooperative uplink multi-BS reception, enabling effective adaptation to temporal channel variations.
- We develop a deep reinforcement learning (DRL) framework to jointly select cooperative BS sets and precoding matrices for each UE location, thereby reducing the complexity of multi-BS coordination and avoiding intensive computational overhead.
- To enhance the effectiveness of the DRL proposed framework, we employ a diffusion model to generate approximate precoding matrices and MIMO streams across different BS sets in the spatial domain, thus improving the overall performance of cooperative multi-BS reception.
- Simulation results based on the comprehensive Vienna Link-Level Simulator [26] demonstrate that the proposed feedback-free uplink multi-BS reception scheme significantly improves spectral efficiency by 17.3%.

The remainder of this paper is organized as follows. Section II reviews the related work. Section III introduces the system model. Section IV details the solution. Simulation results are provided in Section V. Finally, Section VI concludes the paper.

II. Related Work

Cooperative multi-BS reception enables multiple distributed BSs to coherently aggregate UE signals, thereby enhancing the received signal strength without increasing the UE transmit power [27]. Extensive research has been conducted on leveraging multi-BS coordination to improve spectral efficiency and network capacity. For instance, Ngo et al. [28] evaluated the achievable throughput of 5G small-cell and multi-BS coordination within massive MIMO systems, demonstrating that the coordinated architecture yields several-fold performance gains over conventional small-cell deployments. In the context of cooperative multi-BS reception, Björnson et al. [29] derived analytical expressions for uplink spectral efficiency using centralized minimum mean square error (MMSE) combining technology. Although the centralized coordination can achieve optimal performance, it introduces high complexity and heavy fronthaul burden due to the involvement of all BSs. To alleviate this situation, cooperative BS sets were introduced in [30] to mitigate the complexity by limiting the number of active BSs, significantly reducing coordination overhead at the cost of a slight performance loss in spectral efficiency.

However, realizing the performance gains of multi-BS reception relies critically on real-time CSI feedback. In current 5G networks, where CSI is typically updated every 1 ms [31], computing physical layer transmission parameters based on instantaneous CSI imposes substantial communication and computational overhead, particularly in scenarios involving more extensive BS cooperation. Recent research has focused on exploiting statistical CSI instead of real-time feedback for BS coordination. Shi et al. [32] proposed a statistical channel gain matrix-based framework to maximize ergodic sum-rate of multi-BS reception. Similarly, Wang et al. [33] developed closed-form expressions for achievable SINR and optimal precoding scheme leveraging statistical channel correlations. However, such statistical CSI approaches inherently face challenges in accurately determining practical link adaptation parameters, such as the number of MIMO streams and MCS. Additionally, Jiang et al. [34] exploits large-scale fading coefficients to opportunistically select a subset of BSs based on an average channel gain threshold. Nevertheless, due to the dynamic nature of large-scale fading, the cooperative BS set requires periodic recalculations, thus introducing additional computational and coordination overhead.

Depart from statistical CSI-based approaches, recent studies have investigated the use of advanced AI techniques to determine fixed physical layer transmission parameters [35], [36], [37].

Wang et al. [38] proposed a deep learning-based radio map that directly maps user locations to beamforming vectors, which effectively eliminates the requirement for instantaneous CSI acquisition. Liu et al. [39] introduced a VAE-based GenAI model that generates time-domain representative precoders by learning from historical channel data, enabling robust adaptation to temporal channel dynamics. Furthermore, Liu et al. [23] employed a vector-quantized VAE (VQ-VAE) and a conditional diffusion model to generate representative channels from user location embeddings, supporting both single-BS and multi-BS cooperative transmission scenarios. Simulation results demonstrate an improvement of more than 10% in spectral efficiency over conventional statistical CSI-based precoding schemes. Nonetheless, while GAI-based methods have exhibited superior adaptability to time-varying channels, existing studies still fall short of providing a comprehensive physical layer design, particularly with respect to the joint determination of MIMO streams, MCS, and BS sets for cooperative multi-BS reception.

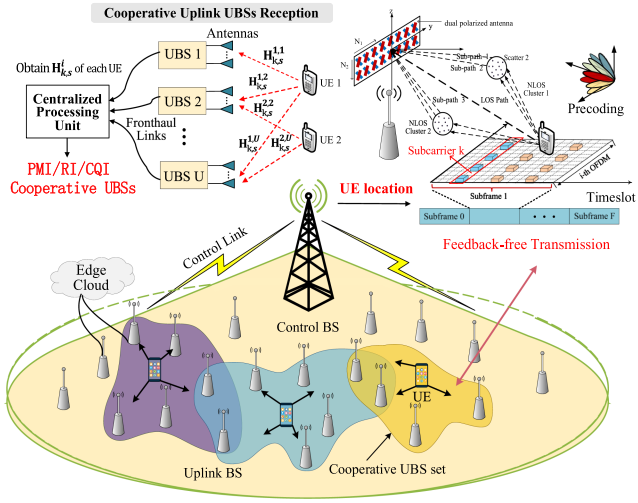

Fig. 1. Cooperative uplink base station reception in FD-RAN.

III. System Model

In this section, we introduce the channel model and present the overall process of cooperative multi-BS reception within the context of the CSI feedback-free mechanism.

A. Three-Dimensional Channel Model

In this paper, the UE wireless signal propagation is modeled in a three-dimensional (3D) space. Compared with traditional two-dimensional channel models, the 3D channel model takes into account the effects of signal propagation in both horizontal and vertical directions, thereby more accurately characterizing the propagation properties in real-world environments [40]. Consider that the UE is equipped with N_{tx} transmitting antennas and the uplink base station (UBS) is equipped with N_{rx} receiving antennas, with the distance of adjacent antennas denoted as d_{H}. Define the set of UEs as $\mathcal{I} = \{1, \ldots, I\}$ and the set of UBSs as $\mathcal{U} = \{1, \ldots, U\}$. For different subcarriers $k \in \mathcal{K} = \{1, \ldots, K\}$ on orthogonal frequency division multiplexing (OFDM) symbol $s \in \mathcal{S} = \{1, \ldots, S\}$, the channel matrix $\mathbf{H}_{k,s}^{i,u} \in \mathbb{C}^{N_{\text{rx}} \times N_{\text{tx}}}$ between UE $i \in \mathcal{I}$ and UBS $u \in \mathcal{U}$ is represented as:

$$\mathbf{H}_{k,s}^{i,u} = \sum_{p=1}^{N_p} \sqrt{\frac{\rho_{k,s}^{i,u,p}}{K}} e^{j\left(\varphi_{k,s}^{i,u,p} + \frac{2\pi k}{K} \tau_{k,s}^{i,u,p} B_w\right)} \mathbf{a}_{BS}\left(\phi_{\text{az}}^{u,p}, \phi_{\text{el}}^{u,p}\right) \mathbf{a}_{UE}^{\text{H}}\left(\phi_{\text{az}}^{i,p}, \phi_{\text{el}}^{i,p}\right), \forall k \in \mathcal{K}, \forall s \in \mathcal{S}, \forall i \in \mathcal{I}, \forall u \in \mathcal{U}, \tag{1}$$

where N_p represents the total number of channel propagation paths between UE i and UBS u. B_w denotes the transmission bandwidth. $\rho_{k,s}^{i,u,p}$, $\varphi_{k,s}^{i,u,p}$ and $\tau_{k,s}^{i,u,p}$ represent the power, phase, and delay of the p-th path, respectively. $\mathbf{a}_{BS}(\phi_{\text{az}}^{u,p}, \phi_{\text{el}}^{u,p})$ and $\mathbf{a}_{UE}(\phi_{\text{az}}^{i,p}, \phi_{\text{el}}^{i,p})$ are the array antenna responses of the UBS and UE, where $\phi_{\text{az}}^{u/i,p}$ and $\phi_{\text{el}}^{u/i,p}$ represent the azimuth angle and elevation angle, respectively. The mathematical expression of the array antenna response for the UBS is defined as:

$$\mathbf{a}_{BS}\left(\phi_{\text{az}}^{u,p}, \phi_{\text{el}}^{u,p}\right) = \mathbf{a}_x\left(\phi_{\text{az}}^{u,p}, \phi_{\text{el}}^{u,p}\right) \otimes \mathbf{a}_y\left(\phi_{\text{az}}^{u,p}, \phi_{\text{el}}^{u,p}\right), \tag{2}$$

in which $\otimes$ denotes the Kronecker product. $\mathbf{a}_x(\cdot)$ and $\mathbf{a}_y(\cdot)$ represent the horizontal and vertical array impulse response vectors for the UBS, respectively. Assume that the horizontal antenna number of the UBS is N_1 and the vertical antenna number is N_2, $\mathbf{a}_x(\cdot)$ and $\mathbf{a}_y(\cdot)$ are expressed as follows:

$$\mathbf{a}_x\left(\phi_{\text{az}}^{u,p}, \phi_{\text{el}}^{u,p}\right) = \left[1, e^{j2\pi d_{\text{H}} \sin\left(\phi_{\text{el}}^{u,p}\right) \cos\left(\phi_{\text{az}}^{u,p}\right)}, \ldots, e^{j2\pi d_{\text{H}}(N_1-1) \sin\left(\phi_{\text{el}}^{u,p}\right) \cos\left(\phi_{\text{az}}^{u,p}\right)}\right]^{\text{T}}, \tag{3}$$

$$\mathbf{a}_y\left(\phi_{\text{az}}^{u,p}, \phi_{\text{el}}^{u,p}\right) = \left[1, e^{j2\pi d_{\text{H}} \sin\left(\phi_{\text{el}}^{u,p}\right) \sin\left(\phi_{\text{az}}^{u,p}\right)}, \ldots, e^{j2\pi d_{\text{H}}(N_2-1) \sin\left(\phi_{\text{el}}^{u,p}\right) \sin\left(\phi_{\text{az}}^{u,p}\right)}\right]^{\text{T}}. \tag{4}$$

Note that the calculation for the UE array antenna response $\mathbf{a}_{UE}(\phi_{\text{az}}^{i,p}, \phi_{\text{el}}^{i,p})$ in (1) follows the same procedure as that in (2)–(4).

B. Cooperative Uplink Reception

For multi-stream data transmission in MIMO-OFDM system, define $\mathbf{s}_{k,s}^{i} \in \mathbb{C}^{L_i \times 1}$ as the L_i-stream transmit data and $\mathbf{y}_{k,s}^{i,u} \in \mathbb{C}^{N_{\text{rx}} \times 1}$ as the signal from UE i to UBS u at the k-th subcarrier on s-th ODFM symbol, which can be expressed as:

$$\mathbf{s}_{k,s}^{i} = \left[s_{k,s}^{i}[1], \ldots, s_{k,s}^{i}[L_i]\right]^{\text{T}}, \tag{5}$$

$$\mathbf{y}_{k,s}^{i,u} = \left[y_{k,s}^{i,u}[1], \ldots, y_{k,s}^{i,u}[N_{\text{rx}}]\right]^{\text{T}}. \tag{6}$$

Since the number of independent spatial streams is limited by the rank of the channel matrix [41], the data streams L_i should not exceed the minimum number of the UBS receive antenna N_{rx} and the UE transmit antenna N_{tx} [42] as:

$$1 \leq L_i \leq \min\left(N_{\text{tx}}, N_{\text{rx}}\right), \forall i \in \mathcal{I}. \tag{7}$$

As shown in Fig. 1, different UBSs will jointly receive the signal from a UE and the cooperative UBS reception set for UE i is defined as $\mathcal{U}_i$. We use a binary variable $x_{i,u}$ to denote the connected association between UE i and UBS u. $x_{i,u}=1$ indicates that UE i is connected to UBS u and $x_{i,u}=0$ otherwise, which are represented as:

$$x_{i,u}=\begin{cases}1 & \text{if UE } i \text{ is connected to UBS } u,\\ 0 & \text{otherwise}\end{cases} \tag{8}$$

Define $\mathbf{X}_{i,u}\in\mathbb{C}^{N_{\text{rx}}\times N_{\text{rx}}}$ as:

$$\mathbf{X}_{i,u}=x_{i,u}\mathbf{I}_{N_{\text{rx}}},\forall i\in\mathcal{I},u\in\mathcal{U}, \tag{9}$$

we can obtain the following joint multi-BS uplink received signal for UE i:

$$\underbrace{\begin{bmatrix}\mathbf{y}_{k,s}^{i,1}\\ \vdots\\ \mathbf{y}_{k,s}^{i,U}\end{bmatrix}}_{\mathbf{y}_{k,s}^{i}\in\mathbb{C}^{N_i N_{\text{rx}}\times 1}}=\underbrace{\begin{bmatrix}\mathbf{X}_{i,1}\mathbf{H}_{k,s}^{i,1}\\ \vdots\\ \mathbf{X}_{i,U}\mathbf{H}_{k,s}^{i,U}\end{bmatrix}}_{\mathbf{X}_i\mathbf{H}_{k,s}^{i}\in\mathbb{C}^{N_i N_{\text{rx}}\times N_{\text{tx}}}}\underbrace{\mathbf{W}_i\mathbf{s}_{k,s}^{i}}_{\in\mathbb{C}^{N_{\text{tx}}\times 1}}+\underbrace{\begin{bmatrix}\mathbf{X}_{i,1}\mathbf{n}_{k,s}^{i,1}\\ \vdots\\ \mathbf{X}_{i,U}\mathbf{n}_{k,s}^{i,U}\end{bmatrix}}_{\mathbf{n}_{k,s}^{i}\in\mathbb{C}^{N_i N_{\text{rx}}\times 1}}, \tag{10}$$

where $\mathbf{H}_{k,s}^{i,u}\in\mathbb{C}^{N_{\text{rx}}\times N_{\text{tx}}}$ is the channel between UE i and UBS u at the k-th subcarrier of OFDM symbol s. $\mathbf{W}_i\in\mathbb{C}^{N_{\text{tx}}\times L_i}$ is the precoding matrix used by UE i to map L_i-stream transmit data $\mathbf{s}_{k,s}^{i}$ into N_{tx} antenna ports. $\mathbf{n}_{k,s}^{i,u}\sim\mathcal{CN}(0,\sigma^2\mathbf{I}_{N_{\text{rx}}})\in\mathbb{C}^{N_{\text{rx}}\times 1}$ is the received additive white Gaussian noise (AWGN) with the covariance matrix denoted as $\sigma^2\mathbf{I}_{N_{\text{rx}}}$. For UE i, the number of UBSs that cooperatively receive the UE signal is indicated by $N_i=|\mathcal{U}_i|$. Define $\mathbf{X}_i\in\mathbb{C}^{N_i N_{\text{rx}}\times N_i N_{\text{rx}}}$ and $\mathbf{H}_{k,s}^{i}\in\mathbb{C}^{N_i N_{\text{rx}}\times N_{\text{tx}}}$ as:

$$\mathbf{X}_i=\text{diag}\left(\left[\mathbf{X}_{i,1},\ldots,\mathbf{X}_{i,U}\right]\right), \tag{11}$$

$$\mathbf{H}_{k,s}^{i}=\left[\mathbf{H}_{k,s}^{i,1},\ldots,\mathbf{H}_{k,s}^{i,U}\right]^{\text{T}}. \tag{12}$$

Therefore, (10) can be transformed into

$$\mathbf{y}_{k,s}^{i}=\mathbf{X}_i\mathbf{H}_{k,s}^{i}\mathbf{W}_i\mathbf{s}_{k,s}^{i}+\mathbf{n}_{k,s}^{i}, \tag{13}$$

where $\mathbf{y}_{k,s}^{i}=[\mathbf{y}_{k,s}^{i,1},\ldots,\mathbf{y}_{k,s}^{i,U}]^{\text{T}}$ and $\mathbf{n}_{k,s}^{i}=[\mathbf{n}_{k,s}^{i,1},\ldots,\mathbf{n}_{k,s}^{i,U}]^{\text{T}}$ represent the received signal vector and noise vector, respectively, from all the UBSs in the cooperative set of UE i.

C. Joint Uplink Channel Equalization

After the UBSs cooperatively receive the signal $\mathbf{y}_{k,s}^{i}$ from UE i, the received signal will be sent to an edge cloud for joint channel equalization, which can reverse the channel effects and recover the received signal to its original transmitted form. In this paper, the commonly used zero-forcing (ZF) equalizer is exploited to perform the channel equalization process. Denote the effective channel matrix $\mathbf{H}_{\text{eff}}\in\mathbb{C}^{N_i N_{\text{rx}}\times L_i}$ as follows:

$$\mathbf{H}_{\text{eff}}=\mathbf{X}_i\mathbf{H}_{k,s}^{i}\mathbf{W}_i=\begin{bmatrix}\mathbf{X}_{i,1}\mathbf{H}_{k,s}^{i,1}\\ \vdots\\ \mathbf{X}_{i,U}\mathbf{H}_{k,s}^{i,U}\end{bmatrix}\mathbf{W}_i. \tag{14}$$

Then the ZF equalizer can be calculated by taking the pseudo inverse of the effective channel matrix as:

$$\begin{aligned}\mathbf{E}_{k,s}^{i}&=\left(\mathbf{H}_{\text{eff}}^{\text{H}}\mathbf{H}_{\text{eff}}\right)^{-1}\mathbf{H}_{\text{eff}}^{\text{H}}\\&=\left(\left(\mathbf{X}_i\mathbf{H}_{k,s}^{i}\mathbf{W}_i\right)^{\text{H}}\mathbf{X}_i\mathbf{H}_{k,s}^{i}\mathbf{W}_i\right)^{-1}\left(\mathbf{X}_i\mathbf{H}_{k,s}^{i}\mathbf{W}_i\right)^{\text{H}},\end{aligned} \tag{15}$$

in which $\mathbf{E}_{k,s}^{i}\in\mathbb{C}^{L_i\times N_i N_{\text{rx}}}$ is the ZF equalizer for the k-th subcarrier of OFDM symbol s and $(\cdot)^{\text{H}}$ represents the Hermitian transpose operation. Subsequently, the received signal $\mathbf{y}_{k,s}^{i}$ will be filtered with equalizer $\mathbf{E}_{k,s}^{i}$ to obtain the post-equalization vector $\widetilde{\mathbf{y}}_{k,s}^{i}\in\mathbb{C}^{L_i\times 1}$:

$$\begin{aligned}\widetilde{\mathbf{y}}_{k,s}^{i}&=\mathbf{E}_{k,s}^{i}\mathbf{y}_{k,s}^{i}\\&=\mathbf{E}_{k,s}^{i}\left(\mathbf{X}_i\mathbf{H}_{k,s}^{i}\mathbf{W}_i\mathbf{s}_{k,s}^{i}+\mathbf{n}_{k,s}^{i}\right)\\&=\underbrace{\mathbf{E}_{k,s}^{i}\mathbf{X}_i\mathbf{H}_{k,s}^{i}\mathbf{W}_i}_{\in\mathbb{C}^{L_i\times L_i}}\mathbf{s}_{k,s}^{i}+\underbrace{\mathbf{E}_{k,s}^{i}\mathbf{n}_{k,s}^{i}}_{\in\mathbb{C}^{L_i\times 1}}.\end{aligned} \tag{16}$$

Let

$$\mathbf{V}_{k,s}^{i}=\mathbf{E}_{k,s}^{i}\mathbf{X}_i\mathbf{H}_{k,s}^{i}\mathbf{W}_i, \tag{17}$$

the post-equalized signal-to-interference-plus-noise-ratio (SINR) for l-th data stream is calculated by

$$\begin{aligned}&\text{P\_SINR}_{k,s,l}^{i}\left(\mathbf{W}_i,\mathbf{X}_i\right)\\&=\frac{\left|\mathbf{V}_{k,s}^{i}\left[l,l\right]\right|^2}{\sum_{l'\neq l}\left|\mathbf{V}_{k,s}^{i}\left[l,l'\right]\right|^2+\sigma^2\sum_{\text{rx}}\left|\mathbf{E}_{k,s}^{i}\left[l,\text{rx}\right]\right|^2},\end{aligned} \tag{18}$$

where $l,l'\in\{1,\ldots,L_i\}$, and $\mathbf{V}_{k,s}^{i}[l,l]$ is the element in the l-th row and l-th column of $\mathbf{V}_{k,s}^{i}$, similarly for $\mathbf{V}_{k,s}^{i}[l,l']$ and $\mathbf{E}_{k,s}^{i}[l,\text{rx}]$. Note that the precoding matrix has the function to map L_i streams of data into transmit symbols, therefore, L_i can be derived as the rank of the precoding matrix as follows:

$$L_i=\text{rank}\left(\mathbf{W}_i\right),\forall\mathbf{W}_i\in\mathcal{P},\forall i\in\mathcal{I}, \tag{19}$$

in which $\mathcal{P}=\{\mathcal{P}_l\}_{l=1}^{L}$ denotes the predefined set of precoding matrices and $\mathcal{P}_l$ is the precoding matrix set for the l-th streams, with L being the predefined maximum stream number.

D. Calculation of Transmission Parameters

To obtain the optimal precoding matrix $\mathbf{W}_i^*$ and transmit stream L_i^* for cooperative UBS reception, mutual information [43], which sums up the post-equalized communication rates of all L_i streams, is introduced and expressed as:

$$\begin{aligned}R_{k,s}^{i}&=\sum_{l=1}^{L_i}\log_2\left(1+\text{P\_SINR}_{k,s,l}^{i}\left(\mathbf{W}_i,\mathbf{X}_i\right)\right)=\sum_{l=1}^{L_i}\log_2\\&\times\left(1+\frac{\left|\mathbf{V}_{k,s}^{i}\left[l,l\right]\right|^2}{\sum_{l'\neq l}\left|\mathbf{V}_{k,s}^{i}\left[l,l'\right]\right|^2+\sigma^2\sum_{\text{rx}}\left|\mathbf{E}_{k,s}^{i}\left[l,\text{rx}\right]\right|^2}\right).\end{aligned} \tag{20}$$

Consequently, once the optimal UE-UBS association $\mathbf{X}_i^*$ is given, the main principle for finding the optimal precoding

matrix is to maximize the mutual information $R_{k,s}^{i}$ over K subcarriers and S OFDM symbols, represented by

$$\begin{aligned}\mathbf{W}_i{}^{*} &= \arg\max \sum_{k=1}^{K}\sum_{s=1}^{S} R_{k,s}^{i}\left(\mathbf{W}_i;\mathbf{X}_i^{*}\right)\\ &= \arg\max \sum_{l=1}^{L_i}\sum_{k=1}^{K}\sum_{s=1}^{S} \log_2\left(1+\mathrm{P\_SINR}_{k,s,l}^{i}\left(\mathbf{W}_i;\mathbf{X}_i^{*}\right)\right).\end{aligned} \tag{21}$$

Afterwards, the optimal transmit stream ${L_i}^{*}$ is obtained as:

$${L_i}^{*} = \mathrm{rank}\left(\mathbf{W}_i^{*}\right), \forall i \in \mathcal{I}. \tag{22}$$

For the determination of CQI in the cooperative uplink UBS reception scenario, we adopt the single UE-UBS association approach that utilizes the exponential effective SINR mapping (ESM) method to convert multiple post-equalized SINR measurements into an equivalent signal-to-noise-ratio (SNR) of a single-input-single-output (SISO) AWGN channel as

$$\mathrm{SNR} = -\zeta \ln\left(\frac{1}{M}\sum_{\mathrm{m}=1}^{M}\exp\left(-\frac{\mathrm{P\_SINR}_m}{\zeta}\right)\right), \tag{23}$$

where M is the total number of post-equalized SINR measurements for the subcarrier and OFDM symbol of interest. ζ is a set of calibrated parameters that correspond to the alphabets of different modulation and coding rates. Therefore, for a subframe duration consisting of L_i data stream, K subcarriers, and S OFDM symbols, the effective SNR is calculated by

$$\begin{aligned}&\mathrm{SNR}_{\mathrm{sub}} = -\zeta\\ &\ln\left(\frac{1}{L_i K S}\sum_{l=1}^{L_i}\sum_{k=1}^{K}\sum_{s=1}^{S}\exp\left(-\frac{\mathrm{P\_SINR}_{k,s,l}^{i}\left(\mathbf{W}_i^{*},\mathbf{X}_i^{*}\right)}{\zeta}\right)\right).\end{aligned} \tag{24}$$

Finally, the optimal CQI^{*} is obtained through the mapping of the maximum $\mathrm{SNR}_{\mathrm{sub}}$ that achieves a block error rate (BLER) of less than 0.1, which can be expressed as:

$$\mathrm{CQI}^{*} \xleftarrow{\text{mapping}} \underset{\mathrm{SNR}_{\mathrm{sub}}}{\arg\max}\left\{\mathrm{SNR}_{\mathrm{sub}} \mid \mathrm{BLER}\left(\mathrm{SNR}_{\mathrm{sub}}\right) \le 0.1\right\}. \tag{25}$$

E. Problem Formulation

For cooperative multi-BS reception, UE throughput depends on the transmission parameters including PMI, RI, CQI, and $\mathbf{X}_i$, which are used to select the precoding matrix, MIMO streams, MCS, and cooperative UBS set. Rather than dynamically adjusting these parameters across different time subframes, we employ time-invariant PMI, RI, CQI, and $\mathbf{X}_i$ to avoid the significant computation overhead of CSI feedback. The overall objective is to obtain optimal time-invariant parameters to maximize the expectation of UE throughput over different time-varying channels, which can be defined as:

$$\max_{\mathbf{W}_i,L_i,x_{i,u}} \mathbb{E}\left(\sum_{k=1}^{K}\sum_{s=1}^{S} R_{k,s}^{i}\right) \triangleq \frac{1}{F}\sum_{f=1}^{F}\sum_{k=1}^{K}\sum_{s=1}^{S} R_{k,s,f}^{i}, \tag{26}$$

where $R_{k,s,f}^{i}$ is the mutual information of the k-th subcarrier and s-th OFDM symbol at the f-th subframe time duration. For a total number of F time-varying subframes, we formulate the feedback-free cooperative uplink reception problem as:

$$\max_{\mathbf{W}_i,L_i,x_{i,u}} \frac{1}{F}\sum_{f=1}^{F}\sum_{l=1}^{L_i}\sum_{k=1}^{K}\sum_{s=1}^{S}\log_2\left(1+\mathrm{P\_SINR}_{k,s,l,f}^{i}\right)$$

$$\text{s.t. } \mathbf{W}_i \in \mathcal{P}_l, \quad \forall i \in \mathcal{I}, 1 \le l \le L, \tag{27a}$$

$$\|\mathbf{W}_i\|_F = 1, \quad \forall i \in \mathcal{I}, \tag{27b}$$

$$\mathrm{rank}\left(\mathbf{W}_i\right) = L_i, \quad \forall i \in \mathcal{I}, \tag{27c}$$

$$1 \le L_i \le \min\left(N_{\mathrm{tx}}, N_{\mathrm{rx}}\right), \quad \forall i \in \mathcal{I} \tag{27d}$$

$$\sum_{u\in\mathcal{U}} x_{i,u} \le N_b, \quad \forall i \in \mathcal{I}, \forall u \in \mathcal{U}, \tag{27e}$$

$$x_{i,u} \in \{0,1\}, \quad \forall i \in \mathcal{I}, \forall u \in \mathcal{U}, \tag{27f}$$

The constraint (27a) in the formulated problem ensures that the precoding matrices used by UEs belong to the predefined precoding set. Constraint (27b) normalizes the precoding matrices into unit power, with the operation $||\cdot||_F$ denoted as the Frobenius norm. Constraint (27c) guarantees the number of data streams equals the rank of the precoding matrix, which is also bounded by the minimum number of transmit and receive antennas as specified in constraint (27d). Constraint (27e) sets the maximum number of cooperative UBSs for a single UE as N_b and constraint (27f) indicates the association between a UE and the UBSs. The optimization problem of (27) will determine the time-invariant PMI, RI, and UBS set, which are then used in the calculation of CQI based on (23)–(25) for realizing the cooperative uplink feedback-free transmission.

IV. Proposed Solution

Given the stochastic characteristics of the wireless channel across different subframes and the presence of binary variables in both the numerator and denominator of the post-equalized SINR, (27) can be regarded as a stochastic mixed-integer programming problem [44]. Such an optimization problem has been demonstrated to be non-convex and non-deterministic polynomial-time hard (NP-hard) [45], making it challenging to obtain a global optimal solution. Nonetheless, channels at one location exhibit high correlation in the spatial, frequency, and time domains. Therefore, in this section, we first employ unsupervised learning with a conditional VAE to generate a representative channel $\widetilde{\mathbf{H}}_{k,s}^{i}$ for subcarrier k, OFDM symbol s, and UE location i using historical F subframe channels as data input, represented by

$$\widetilde{\mathbf{H}}_{k,s}^{i} = \mathrm{CVAE}\left(\{\mathbf{H}_{k,s,f}^{i}\}_{f=1}^{F}\right), \forall k \in \mathcal{K}, \forall s \in \mathcal{S}, \forall i \in \mathcal{I}. \tag{28}$$

The representative channel is trained and obtained with the aim of learning the distribution of the input data, thereby effectively adapting to the F dynamically changing subframe channels. Consequently, by substituting the F subframe channels with a single representative channel, the stochastic property of formulation (27) is eliminated, transforming it into the following

problem

$$\max_{\mathbf{w}_i, L_i, x_{i,u}} \sum_{l=1}^{L_i} \sum_{k=1}^{K} \sum_{s=1}^{S} \log_2 \left(1 + \text{P\_SINR}_{k,s,l}^{i} \left(\widetilde{\mathbf{H}}_{k,s}^{i}\right)\right)$$
$$\text{s.t. (27a)} - \text{(27f)}. \tag{29}$$

Problem (29) targets at obtaining the optimal PMI, RI, and UBS set for cooperative uplink transmission under the given representative channel matrix $\widetilde{\mathbf{H}}_{k,s}^{i}$. Due to the complexity of large-scale mixed-integer programming in dealing with various UBS cooperation schemes, we employ a diffusion model based DRL framework to generate the UBS cooperation set and the precoding decisions based on the UE location, thus providing a feasible solution to problem (29) and obtaining the time-invariant parameters in feedback-free transmission.

A. VAE Based Channel Generation

The fundamental basis of VAE is to model the distribution of given channel data $\boldsymbol{h}$ by introducing latent variables $\boldsymbol{z}$. This scheme aims to maximize the marginal likelihood $p(\boldsymbol{h})$ of the channel data to the precisely generate a representative channel. However, directly computing $p(\boldsymbol{h})$ is usually intractable due to the difficulty of implementing the integration over all possible latent variables $\boldsymbol{z}$, which can be expressed as:

$$p(\boldsymbol{h}) = \int p(\boldsymbol{h}, \boldsymbol{z}) d\mathbf{z} = \int p(\boldsymbol{h}|\boldsymbol{z}) p(\boldsymbol{z}) d\boldsymbol{z}. \tag{30}$$

Through denoting the approximated posterior distribution as $q(\boldsymbol{z}|\boldsymbol{h})$, VAE calculates the log of the marginal likelihood

$$\begin{aligned} \log p(\boldsymbol{h}) &= \log \int q(\boldsymbol{z}|\boldsymbol{h}) \frac{p(\boldsymbol{h}, \boldsymbol{z})}{q(\boldsymbol{z}|\boldsymbol{h})} d\boldsymbol{z} \\ &\overset{(1)}{\geq} \int q(\boldsymbol{z}|\boldsymbol{h}) \log \left(\frac{p(\boldsymbol{h}, \boldsymbol{z})}{q(\boldsymbol{z}|\boldsymbol{h})}\right) d\boldsymbol{z} \\ &\overset{(2)}{=} \int q(\boldsymbol{z}|\boldsymbol{h}) \log \left(\frac{p(\boldsymbol{h}|\boldsymbol{z}) p(\boldsymbol{z})}{q(\boldsymbol{z}|\boldsymbol{h})}\right) d\boldsymbol{z}, \end{aligned} \tag{31}$$

where $\overset{(1)}{\geq}$ is based on Jensen's inequality $\log \mathbb{E}[X] \geq \mathbb{E}[\log X]$ and $\overset{(2)}{=}$ follows from the Bayes' rule. Consequently, the VAE maximizes the evidence lower bound (ELBO) of $\log p(\boldsymbol{h})$ in (31) by employing the negative ELBO as the loss function, which can be derived as follows:

$$\begin{aligned} &\mathcal{L}_{ELBO} \\ &= -\int q(\boldsymbol{z}|\boldsymbol{h}) \log p(\boldsymbol{h}|\boldsymbol{z}) d\boldsymbol{z} + \int q(\boldsymbol{z}|\boldsymbol{h}) \log \left(\frac{p(\boldsymbol{z})}{q(\boldsymbol{z}|\boldsymbol{h})}\right) d\boldsymbol{z} \\ &= \underbrace{-\mathbb{E}_{q(\boldsymbol{z}|\boldsymbol{h})} \left[\log p(\boldsymbol{h}|\boldsymbol{z})\right]}_{Reconstruction\ Loss} + \underbrace{D_{\text{KL}}(q(\boldsymbol{z}|\boldsymbol{h}) \| p(\boldsymbol{z}))}_{KL\ Divergence}. \end{aligned} \tag{32}$$

The loss function $\mathcal{L}_{ELBO}$ consists of a reconstruction loss that measures the expected log likelihood of the generative distribution $p(\boldsymbol{h}|\boldsymbol{z})$ given latent variables $\boldsymbol{z}$, and the Kullback-Leibler (KL) divergence between the approximated posterior distribution $q(\boldsymbol{z}|\boldsymbol{h})$ and prior distribution $p(\boldsymbol{z})$, typically formulated as a standard normal distribution $\mathcal{N}(\mathbf{0}, \mathbf{I})$. Then, VAE utilizes an encoder ϕ_e to model the approximated posterior distribution $q_{\phi_e}(\boldsymbol{z}|\boldsymbol{h})$, and a decoder ϕ_d to model the generative distribution $p_{\phi_d}(\boldsymbol{h}|\boldsymbol{z})$, thereby minimizing the negative ELBO through the stochastic gradient descent method.

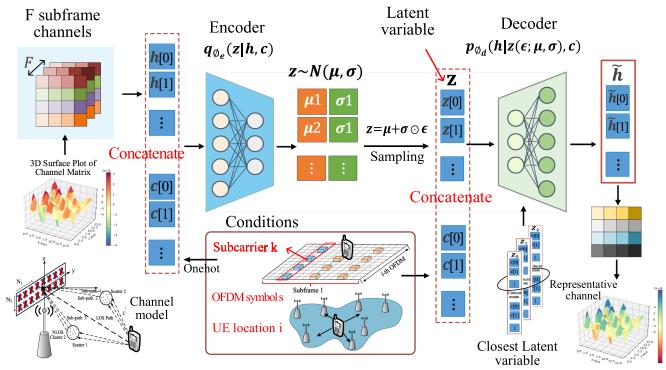

Fig. 2. The structure of conditional variational autoencoder.

Fig. 2 illustrates the proposed CVAE framework to train a representative channel based on the conditional information of subcarrier k, OFDM symbol s, and UE location i. In order to differentiate the various conditions, we introduce the onehot encoding to transform the condition into a vector, where the element of corresponding condition is 1 and all other elements are 0. For instance, the onehot encoding $\text{onehot}(i) \in \mathbb{R}^{1\times I}$ for the UE location i is expressed as:

$$\text{onehot}(i)[i'] = \begin{cases} 1 & \text{if } i' = i \\ 0 & \text{otherwise} \end{cases}, i' = 1, \ldots, I. \tag{33}$$

Subsequently, the onehot vectors of the subcarrier, OFDM symbol, and UE location will be concatenated to form part of the encoder input along with the original channel data, and will also be part of the decoder input along with the latent variables $\boldsymbol{z}$. The concatenated vector $\mathbf{c} \in \mathbb{R}^{KSI}$ is denoted by

$$\begin{aligned} \mathbf{c} = &\left[\text{onehot}(k), \text{onehot}(s), \text{onehot}(i)\right]^{\mathrm{T}}, \\ &\forall k \in \mathcal{K}, \forall s \in \mathcal{S}, \forall i \in \mathcal{I}. \end{aligned} \tag{34}$$

Since the prior distribution $p(\boldsymbol{z})$ follows a standard normal distribution, the posterior distribution $q_{\phi_e}(\boldsymbol{z}|\boldsymbol{h}; \mathbf{c})$ based on a condition vector $\mathbf{c}$ is assumed to be a Gaussian distribution to simplify calculations, with its mean and variance predicted by the encoder network ϕ_e as:

$$q_{\phi_e}(\boldsymbol{z}|\boldsymbol{h}, \mathbf{c}) \sim \mathcal{N}(\boldsymbol{\mu}_{\phi_e}, \boldsymbol{\sigma}_{\phi_e} \mathbf{I}). \tag{35}$$

To enable the gradient back propagation of latent variables $\boldsymbol{z}$ through the sampling process in (35), a reparameterization technique [46] is used to sample $\boldsymbol{z}$ from Gaussian noise:

$$\boldsymbol{z} = \boldsymbol{\mu}_{\phi_e} + \boldsymbol{\sigma}_{\phi_e} \odot \boldsymbol{\epsilon}, \quad \boldsymbol{\epsilon} \sim \mathcal{N}(\mathbf{0}, \mathbf{I}), \tag{36}$$

where $\odot$ is the operation of Hadamard product for element-wise multiplication. Based on [46], the generated channel $\boldsymbol{h} \in \mathbb{R}^{d}$ by

decoder ϕ_d is assumed to be d-dimentiaonal Gaussian distribution as $p_{\phi_d}(\boldsymbol{h}|\boldsymbol{z},\mathbf{c}) \sim \mathcal{N}(\tilde{\boldsymbol{h}}_{\phi_d}, \sigma_h \mathbf{I}_d)$ with a fixed variance σ_h. Therefore, the gradient of the reconstruction loss $\mathcal{L}_{rec}$ in (32) can be transformed into:

$$\begin{aligned}\mathcal{L}_{rec} &= -\mathbb{E}_{q_{\phi_e}(\boldsymbol{z}|\boldsymbol{h},\mathbf{c})}\left[\log p_{\phi_d}(\boldsymbol{h}|\boldsymbol{z},\mathbf{c})\right] \\ &= -\mathbb{E}_{\boldsymbol{\epsilon}\sim\mathcal{N}(\mathbf{0},\mathbf{I})}\left[\log p_{\phi_d}(\boldsymbol{h}|\boldsymbol{z}(\boldsymbol{\epsilon};\boldsymbol{\mu}_{\phi_e},\boldsymbol{\sigma}_{\phi_e}),\mathbf{c})\right] \\ &= \mathbb{E}_{\boldsymbol{\epsilon}\sim\mathcal{N}(\mathbf{0},\mathbf{I})}\left[\frac{1}{2\sigma_h^2}\left\|\boldsymbol{h}-\tilde{\boldsymbol{h}}_{\phi_d}\left(\boldsymbol{z}(\boldsymbol{\epsilon};\boldsymbol{\mu}_{\phi_e},\boldsymbol{\sigma}_{\phi_e}),\mathbf{c}\right)\right\|^2\right. \\ &\quad \left.+\frac{d}{2}\log(2\pi)+\frac{d}{2}\log\left(\sigma_h^2\right)\right] \\ &\overset{(3)}{\simeq} \frac{1}{2\sigma_h^2 N_s}\sum_{n=1}^{N_s}\left\|\boldsymbol{h}^{(n)}-\tilde{\boldsymbol{h}}_{\phi_d}^{(n)}\left(\boldsymbol{z}(\boldsymbol{\epsilon}^{(n)};\boldsymbol{\mu}_{\phi_e},\boldsymbol{\sigma}_{\phi_e}),\mathbf{c}\right)\right\|^2,\end{aligned} \tag{37}$$

in which N_s is the total number of training channel samples and $\tilde{\boldsymbol{h}}_{\phi_d}$ is the generated representative channel from the decoder network ϕ_d. $\overset{(3)}{\simeq}$ is obtained by dropping the constant term $\frac{d}{2}\log(2\pi)+\frac{d}{2}\log(\sigma_h^2)$ and approximating the remaining expectation with Monte Carlo sampling. This adopted approximation is an unbiased estimator of the original reconstruction loss $\mathcal{L}_{rec}$. Moreover, its variance decreases proportionally to $\mathcal{O}(1/N_s)$, which demonstrates the tightness of the adopted approximation. A detailed proof is provided in as follows.

Proof: Let the Monte Carlo estimator for the original $\mathcal{L}_{rec}$ be:

$$\hat{\mathcal{L}}_{rec} = \frac{1}{2\sigma_h^2 N_s}\sum_{n=1}^{N_s}\left\|\boldsymbol{h}^{(n)}-\tilde{\boldsymbol{h}}_{\phi_d}^{(n)}\left(\boldsymbol{z}(\boldsymbol{\epsilon}^{(n)};\boldsymbol{\mu}_{\phi_e},\boldsymbol{\sigma}_{\phi_e}),\mathbf{c}\right)\right\|^2, \tag{38}$$

Then the expectation of the estimation can be expressed as:

$$\begin{aligned}&\mathbb{E}\left[\hat{\mathcal{L}}_{rec}\right] \\ &= \mathbb{E}_{\boldsymbol{\epsilon}^{(1)},\ldots,\boldsymbol{\epsilon}^{(N_s)}}\left[\frac{1}{2\sigma_h^2 N_s}\sum_{n=1}^{N_s}\left\|\boldsymbol{h}^{(n)}-\tilde{\boldsymbol{h}}_{\phi_d}^{(n)}\left(\boldsymbol{z}(\boldsymbol{\epsilon}^{(n)}),\mathbf{c}\right)\right\|^2\right] \\ &= \frac{1}{N_s}\sum_{n=1}^{N_s}\mathbb{E}_{\boldsymbol{\epsilon}^{(n)}\sim\mathcal{N}(\mathbf{0},\mathbf{I})}\left[\frac{1}{2\sigma_h^2}\left\|\boldsymbol{h}^{(n)}-\tilde{\boldsymbol{h}}_{\phi_d}^{(n)}\left(\boldsymbol{z}(\boldsymbol{\epsilon}^{(n)}),\mathbf{c}\right)\right\|^2\right] \\ &= \frac{1}{N_s}\sum_{n=1}^{N_s}\mathbb{E}_{q_{\phi_e}(\boldsymbol{z}|\boldsymbol{h}^{(n)},\mathbf{c})}\left[\frac{1}{2\sigma_h^2}\left\|\boldsymbol{h}^{(n)}-\tilde{\boldsymbol{h}}_{\phi_d}^{(n)}\left(\boldsymbol{z},\mathbf{c}\right)\right\|^2\right] \\ &= \frac{1}{N_s}\sum_{n=1}^{N_s}\left(-\mathbb{E}_{q_{\phi_e}(\boldsymbol{z}|\boldsymbol{h}^{(n)},\mathbf{c})}\left[\log p_{\phi_d}(\boldsymbol{h}|\boldsymbol{z},\mathbf{c})\right]\right) = \mathcal{L}_{rec},\end{aligned} \tag{39}$$

Thus, the estimator is an unbiased Monte Carlo estimator of the true reconstruction loss. For the tightness of approximation, let the per-sample reconstruction error be:

$$R^{(n)}(\boldsymbol{\epsilon}) = \frac{1}{2\sigma_h^2}\left\|\boldsymbol{h}^{(n)}-\tilde{\boldsymbol{h}}_{\phi_d}^{(n)}\left(\boldsymbol{z}(\boldsymbol{\epsilon}^{(n)}),\mathbf{c}\right)\right\|^2, \tag{40}$$

Algorithm 1: CVAE for Representative Channel Generation.

Input: Original N_f subframe channels $\{\mathbf{H}_{k,s,f}^i\}_{f=1}^F$.
Output: Representative channel matrix $\widetilde{\mathbf{H}}_{k,s}^i$.
Flatten original channel matrix into channel vector $\boldsymbol{h}$,
repeat
  Obtain a batch of channel data from $p(\boldsymbol{h})$,
  Compute the concatenated vector $\boldsymbol{c}$ based on the onehot encoding of conditions k, s, and i,
  Sample the latent variables $\boldsymbol{z}$ using the output mean $\boldsymbol{\mu}_{\phi_e}$ and variances $\boldsymbol{\sigma}_{\phi_e}$ from the CVAE encoder and random noise following $q_{\phi_e}(\boldsymbol{z}|\boldsymbol{h},\mathbf{c}) \sim \mathcal{N}(\boldsymbol{\mu}_{\phi_e}, \boldsymbol{\sigma}_{\phi_e}\mathbf{I})$,
  Obtain the reconstructed channel vectors $\tilde{\boldsymbol{h}}_{\phi_d}\left(\boldsymbol{z}(\boldsymbol{\epsilon};\boldsymbol{\mu}_{\phi_e},\boldsymbol{\sigma}_{\phi_e}),\mathbf{c}\right)$ from the CVAE decoder,
  Perform gradient descent with $\mathcal{L}_{ELBO}$ based on Eq. (37) and Eq. (43).
until *The encoder network ϕ_e and decoder network ϕ_d of the CVAE converges*;
Utilization: Select the latent variable with the closest mean value and variance for conditions k, s, and i to generate $\widetilde{\mathbf{H}}_{k,s}^i$ through well-trained CVAE decoder.

Then, the variance of per sample is calculated by:

$$\mathrm{Var}\left(R^{(n)}(\boldsymbol{\epsilon})\right) = \frac{1}{4\sigma_h^4}\mathrm{Var}_{\boldsymbol{\epsilon}}\left(\left\|\boldsymbol{h}^{(n)}-\tilde{\boldsymbol{h}}_{\phi_d}^{(n)}\left(\boldsymbol{z}(\boldsymbol{\epsilon}^{(n)}),\mathbf{c}\right)\right\|^2\right). \tag{41}$$

Consequently, the variance of $\hat{\mathcal{L}}_{rec}$ can be expressed as:

$$\begin{aligned}\mathrm{Var}\left(\hat{\mathcal{L}}_{\mathrm{rec}}\right) &= \mathrm{Var}\left(\frac{1}{N_s}\sum_{n=1}^{N_s}R^{(n)}\left(\boldsymbol{\epsilon}^{(n)}\right)\right) \\ &= \frac{1}{N_s^2}\sum_{n=1}^{N_s}\mathrm{Var}\left(R^{(n)}\right) \overset{(4)}{=} \frac{1}{N_s}\mathrm{Var}\left(R^{(n)}\right),\end{aligned} \tag{42}$$

where $\overset{(4)}{=}$ is obtained based on the assumption that all samples are independent and identically distributed (i.i.d.). Therefore, the variance of the adopted approximation in (37) decreases proportionally to $\mathcal{O}(1/N_s)$. □

In addition, the gradient of the KL divergence in (32) can be derived based on the mean values and variances of the two Gaussian distributions:

$$\begin{aligned}&D_{\mathrm{KL}}(q_{\phi_e}(\boldsymbol{z}|\boldsymbol{h}))\|p(\boldsymbol{z})) \\ &= \frac{1}{2}\sum_{n=1}^{N_s}\left(1+\log\left(\boldsymbol{\sigma}_{\phi_e}^2\right)-\boldsymbol{\mu}_{\phi_e}^2-\boldsymbol{\sigma}_{\phi_e}^2\right).\end{aligned} \tag{43}$$

Upon completion of the CVAE training, we use one latent variable to generate a channel matrix that most closely matches the distribution of the original F subframe channels. This latent variable is selected such that its mean value and variance are closest to the average mean value $\overline{\boldsymbol{\mu}}_{\phi_e}$ and variance $\overline{\boldsymbol{\sigma}}_{\phi_e}^2$

corresponding to the F subframes, as expressed by

$$\arg\min_{f\in\{1,\ldots,F\}} \left(\left(\boldsymbol{\mu}_{\phi_e}^{(f)}-\overline{\boldsymbol{\mu}}_{\phi_e}\right)^{\mathrm{T}}\left(\boldsymbol{\mu}_{\phi_e}^{(f)}-\overline{\boldsymbol{\mu}}_{\phi_e}\right) + \left((\boldsymbol{\sigma}_{\phi_e}^{(f)})^2-\overline{\boldsymbol{\sigma}}_{\phi_e}^2\right)^{\mathrm{T}}\left((\boldsymbol{\sigma}_{\phi_e}^{(f)})^2-\overline{\boldsymbol{\sigma}}_{\phi_e}^2\right)\right). \quad (44)$$

Finally, we present the detailed procedures of the proposed CVAE approach for generating representative channel matrices in **Algorithm 1**. For a given set of F subframe channels $\{\mathbf{H}_{k,s,f}^i\}_{f=1}^F$, we first flatten $\mathbf{H}_{k,s,f}^i$ into channel vector $\boldsymbol{h}$ and compute the onehot conditional vector $\boldsymbol{c}$ base on k, s, and i. The conditional vector serves as the input to both the CVAE encoder and decoder networks. After training the CVAE, a selected latent variable based on (44) is used by the CVAE decoder to generate the desired representative channel $\widetilde{\mathbf{H}}_{k,s}^i$.

The proposed algorithm optimizes the ELBO through the stochastic gradient descent (SGD). Since the reconstruction loss $\mathcal{L}rec$ is approximated as a mean-squared error (MSE) form in (37), and the KL divergence possesses a closed-form expression as given in (43), the overall ELBO is a smooth and continuously differentiable function with respect to the encoder parameters ϕ_e and the decoder parameters ϕ_d. Based on non-convex stochastic optimization theory [47], the algorithm is guaranteed to converge to a first-order stationary point at a rate of $\mathcal{O}(1/\sqrt{T_c})$, where T_c denotes the total number of iterations. The complexity of Algorithm 1 scales linearly with both the data size and the model size. Specifically, each training iteration requires $\mathcal{O}(N_s(\zeta_{\text{enc}}+\zeta_{\text{dec}}))$ operations, where ζ_{enc} and ζ_{dec} denote the forward computational costs of the encoder and decoder networks, respectively. Therefore, for training over T_c epochs, the total computational complexity is given by $\mathcal{O}(T_cN_s(\zeta_{\text{enc}}+\zeta_{\text{dec}}))$.

B. Deep Reinforcement Learning Framework

Since problem (29) involves selecting UBS from $\mathcal{U}$ and precoding matrix from $\mathcal{P}$ for each UE under the calculated representative channel $\widetilde{\mathbf{H}}_{k,s}^i$, the basic principle of employing a DRL framework to solve the problem (29) is to independently output the UBS cooperation schemes and precoding schemes, thus avoiding the intensive joint computation of PMI, RI, and UBS set. The state, action, and reward function of the proposed DRL framework are defined as follows.

1) State: In the scenario of uplink FD-RAN feedback-free cooperative reception mechanism, the time-invariant physical layer parameters are determined exclusively based on the UE's geolocation information. Consequently, the three-dimensional coordinates loc_x, loc_y, loc_z for the horizontal, vertical, and altitude positions of each UE are used as the state information for the DRL framework:

$$\mathbf{s}^i=\left[loc_x^i, loc_y^i, loc_z^i\right]^{\mathrm{T}}, \forall i\in\mathcal{I}. \quad (45)$$

2) Action: The action for solving problem (29) consists of selecting the cooperative UBS set and selecting the precoding matrix for each UE. For the action of selecting UBS set $\mathcal{A}_{\mathcal{U}}^i$, we use the binomial coefficient $\binom{U}{N_i}$ to indicate the choices for UE i to select N_i UBSs from the total U UBSs. Due to the constraint (27e) that bounds the maximum numbers of cooperative UBSs as N_b, N_i should be less than or equal to N_b. The action space for all UBS cooperation schemes under this constraint can be represented by

$$|\mathcal{A}_{\mathcal{U}}^i|=\sum_{N_i=1}^{N_b}\binom{U}{N_i}=\sum_{N_i=1}^{N_b}\frac{U!}{N_i!(U-N_i)!}. \quad (46)$$

For the action of selecting precoding matrix $\mathcal{A}_{\mathcal{P}}^i$, we use the 3GPP type-I codebook $\mathcal{P}^{(\text{type-I})}$ [48] that defines the precoding matrices for different data streams based on the discrete Fourier transform (DFT) beams. Each row of the type-I codebook is formed by DFT beam vectors with a unit norm, thus satisfying the unit power constraint (27b). The DFT beams possess orthogonality and uniform beam directionality, rendering them highly effective for precoding in multi-antenna systems, which are expressed as

$$\mathcal{B}_{n_1}=\left[1\, e^{j\frac{2\pi n_1\cdot 1}{N_1O_1}} e^{j\frac{2\pi n_1\cdot 2}{N_1O_1}}\cdots e^{j\frac{2\pi n_1\cdot(N_1-1)}{N_1O_1}}\right]^{\mathrm{T}}, \quad \forall n_1\in\{0,1,\ldots,O_1N_1-1\}, \quad (47)$$

where N_1 represents the number of horizontal antennas and O_1 denotes the DFT over-sampling factor. Similarly, the DFT beams for the vertical antenna can be attained as $\mathcal{B}_{n_2}, \forall n_2\in\{0,1,\ldots,O_2N_2-1\}$ with N_2 being the vertical antenna number and O_2 being the over-sampling factor. The precoding matrix in type-I codebook is basically calculated in the following mathematical form

$$\mathbf{W}=\mathcal{M}_1\mathcal{M}_2=\begin{bmatrix}\mathcal{B}_{n_1}\otimes\mathcal{B}_{n_2} & 0\\ 0 & \mathcal{B}_{n_1}\otimes\mathcal{B}_{n_2}\end{bmatrix}\mathcal{M}_2, \quad (48)$$

wherein $\mathcal{M}_1$ is a wide-band feedback matrix constructed by the Kronecker product of the horizontal and the vertical DFT beams $\mathcal{B}_{n_1}\otimes\mathcal{B}_{n_2}$. $\mathcal{M}_2$ is a narrow-band feedback matrix that provides a finer granularity of beam adjustment for specific sub-bands. For the codebooks of stream 1,

$$\mathcal{M}_2=\frac{1}{\sqrt{2N_1N_2}}\left[\mathbf{e},\psi_{n_3}\mathbf{e}\right]^{\mathrm{T}}, \psi_{n_3}=e^{j\psi\frac{n_3}{2}}, n_3\in\mathbb{N}_0, \quad (49)$$

with ψ_{n_3} being a co-phasing factor. Let

$$\mathcal{C}_{n_1,n_2}=\mathcal{B}_{n_1}\otimes\mathcal{B}_{n_2}\in\mathbb{C}^{N_1N_2\times 1}, \quad (50)$$

the precoding matrices for stream 1 can be expressed as:

$$\mathbf{W}_{n_1,n_2,n_3}^{(l=1)}=\frac{1}{\sqrt{2N_1N_2}}\begin{bmatrix}\mathcal{C}_{n_1,n_2}\\ \psi_{n_3}\mathcal{C}_{n_1,n_2}\end{bmatrix}. \quad (51)$$

The formulation of type-I codebook for other streams follows the same principles as stream 1. For instance, the detailed expression of the precoding matrices for stream 4 is given by

$$\mathbf{W}_{n_1,n_1',n_2,n_2',n_3}^{(l=4)}=\frac{1}{\sqrt{4\cdot 2N_1N_2}}\begin{bmatrix}\mathcal{C}_{n_1,n_2} & \mathcal{C}_{n_1',n_2'} & \mathcal{C}_{n_1,n_2} & \mathcal{C}_{n_1',n_2'}\\ \psi_{n_3}\mathcal{C}_{n_1,n_2} & \psi_{n_3}\mathcal{C}_{n_1',n_2'} & -\psi_{n_3}\mathcal{C}_{n_1,n_2} & -\psi_{n_3}\mathcal{C}_{n_1',n_2'}\end{bmatrix}, \quad (52)$$

where $n_1, n_1' \in \{0, 1, \ldots, O_1 N_1 - 1\}$ and $n_2, n_2' \in \{0, 1, \ldots, O_2 N_2 - 1\}$. As a consequence, the total number of precoding matrices in the type-I codebook for all data streams forms the action space of $\mathcal{A}_{\mathcal{P}}^i$, which is denoted as:

$$|\mathcal{A}_{\mathcal{P}}^i| = |\mathcal{P}^{(\text{type-I})}| = \sum_{l=1}^{L} |\mathcal{P}_l^{(\text{type-I})}|. \tag{53}$$

Regarding a particular UE in the network, it can arbitrarily select the action of precoding matrix from $\mathcal{P}^{(\text{type-I})}$ as specified in constraint (27a). Due to the orthogonal property of the DFT beams, the rank of the precoding matrix is equal to the number of data streams, thus guaranteeing the satisfaction of constraint (27c). Additionally, since the number of data streams should not exceed the number of transmit or receive antennas, the maximum data stream for precoding matrix selection is set to $\min(N_{\text{tx}}, N_{\text{rx}})$, ensuring compliance with constraint (27d).

3) Reward: Given a specific UE location state $\mathbf{s}^i$, once the action $\mathcal{A}_{\mathcal{U}}^i$ for the UBS set and the action $\mathcal{A}_{\mathcal{P}}^i$ for the precoding matrix are selected, the reward function $\mathcal{R}(\mathbf{s}^i, \mathcal{A}_{\mathcal{U}}^i, \mathcal{A}_{\mathcal{P}}^i)$ is defined as the sum of the post-equalized SINRs corresponding to the representative channel matrix $\widetilde{\mathbf{H}}_{k,s}^i$ generated by CVAE, which is expressed as:

$$\mathcal{R}(\mathbf{s}^i, \mathcal{A}_{\mathcal{U}}^i, \mathcal{A}_{\mathcal{P}}^i) = \sum_{l=1}^{L_i} \sum_{k=1}^{K} \sum_{s=1}^{S} \log_2 \left(1 + \text{P\_SINR}_{k,s,l}^i \left(\widetilde{\mathbf{H}}_{k,s}^i\right)\right). \tag{54}$$

As a consequence, maximizing the reward function leads to the maximization of the objective function within the problem (29). In addition, the binomial coefficient of $\mathcal{A}_{\mathcal{U}}$ to choose no more than N_b UBSs and the precoding matrix selected by $\mathcal{A}_{\mathcal{P}}$ from the type-I codebook, with data streams less than or equal to $\min(N_{\text{tx}}, N_{\text{rx}})$, will satisfy all the constraints (27a)–(27f), thereby providing a feasible solution to problem (29). In the context of the proposed DRL framework, two independent networks $\theta_{\mathcal{U}}$ and $\theta_{\mathcal{P}}$ will output the $\mathcal{Q}$-values for $|\mathcal{A}_{\mathcal{U}}^i|$ UBS cooperation schemes and $|\mathcal{A}_{\mathcal{P}}^i|$ precoding schemes, denoted by $\mathcal{Q}_{\theta_{\mathcal{U}}}(\mathbf{s}^i) = [\mathcal{Q}_{\theta_{\mathcal{U}}}(\mathbf{s}^i, 1), \ldots, \mathcal{Q}_{\theta_{\mathcal{U}}}(\mathbf{s}^i, |\mathcal{A}_{\mathcal{U}}^i|)]^{\text{T}}$ and $\mathcal{Q}_{\theta_{\mathcal{P}}}(\mathbf{s}^i) = [\mathcal{Q}_{\theta_{\mathcal{P}}}(\mathbf{s}^i, 1), \ldots, \mathcal{Q}_{\theta_{\mathcal{P}}}(\mathbf{s}^i, |\mathcal{A}_{\mathcal{P}}^i|)]^{\text{T}}$, respectively. For the selected UBS set $\mathcal{A}_{\mathcal{U}}^i$ and precoding matrix $\mathcal{A}_{\mathcal{P}}^i$ of the UE location state $\mathbf{s}^i$, the loss function of the networks $\theta_{\mathcal{U}}$ and $\theta_{\mathcal{P}}$ are defined as:

$$\mathcal{L}(\theta_{\mathcal{U}}, \theta_{\mathcal{P}}) = \frac{1}{2}\left(\left\|\mathcal{Q}_{\theta_{\mathcal{U}}}(\mathbf{s}^i, \mathcal{A}_{\mathcal{U}}^i) - \mathcal{R}(\mathbf{s}^i, \mathcal{A}_{\mathcal{U}}^i, \mathcal{A}_{\mathcal{P}}^i)\right\|^2 + \left\|\mathcal{Q}_{\theta_{\mathcal{P}}}(\mathbf{s}^i, \mathcal{A}_{\mathcal{P}}^i) - \mathcal{R}(\mathbf{s}^i, \mathcal{A}_{\mathcal{U}}^i, \mathcal{A}_{\mathcal{P}}^i)\right\|^2\right). \tag{55}$$

The network parameters will be updated using the gradient descent method to guarantee the converge of the DRL training process. The updates are performed with learning rates $\gamma_{\mathcal{U}}$ and $\gamma_{\mathcal{P}}$, and are formulated in the following expression

$$\begin{aligned} \theta_{\mathcal{U}} &= \theta_{\mathcal{U}} - \gamma_{\mathcal{U}} \nabla_{\theta_{\mathcal{U}}} \mathcal{L}(\theta_{\mathcal{U}}, \theta_{\mathcal{P}}), \\ \theta_{\mathcal{P}} &= \theta_{\mathcal{P}} - \gamma_{\mathcal{P}} \nabla_{\theta_{\mathcal{P}}} \mathcal{L}(\theta_{\mathcal{U}}, \theta_{\mathcal{P}}). \end{aligned} \tag{56}$$

C. Diffusion Model Enabled Precoding Selection

The proposed DRL framework will independently output the actions $\mathcal{A}_{\mathcal{U}}^i$ and $\mathcal{A}_{\mathcal{P}}^i$ to jointly calculate the reward function and attain a feasible UBS set and precoding matrix for problem (29). Noticed that once the action $\mathcal{A}_{\mathcal{U}}^i$ for the cooperative UBS set is decided, we can iterate all the satisfied precoding matrices in the type-I codebook to obtain $\mathbf{W}_0^i$ that maximizes the reward function based on (21), thus enhancing the overall performance of cooperative multi-BS reception.

Therefore, in this section, we propose utilizing a diffusion model to approximate the iterated optimal precoding matrix $\mathbf{W}_0^i$ for each outputted cooperative UBS set $\mathcal{A}_{\mathcal{U}}^i$. Given the proficiency of the diffusion models in modeling complex data distributions, it is more effective than fully connected layers for handling complex strategy spaces or high-dimensional inputs in DRL tasks. The overall structure of the diffusion model for the precoding selection within the proposed DRL framework is illustrated in Fig. 3.

In the diffusion model enabled precoding matrix selection process, with regard to the optimal precoding matrix $\mathbf{W}_0^i$ for a given cooperative UBS set $\mathcal{A}_{\mathcal{U}}^i$, the diffusion model will perform a forward process to gradually add Gaussian noise to $\mathbf{W}_0^i$, followed by a reverse process to recover the optimal precoding matrix from Gaussian noise. The forward diffusion process will be executed within T time steps and the Gaussian noise is assumed to obey a fixed variance schedule $\beta_t, t \in [0, T]$. To differentiate the optimal precoding matrix across various cooperative UBS schemes, the action $\mathcal{A}_{\mathcal{U}}^i$ will be used as the conditional information for the diffusion model. Consequently, the forward process can be described as:

$$\begin{aligned} q\left(\mathbf{W}_t | \mathbf{W}_{t-1}, \mathcal{A}_{\mathcal{U}}\right) &= q\left(\mathbf{W}_t | \mathbf{W}_{t-1}\right) \\ &= \mathcal{N}\left(\mathbf{W}_t; \sqrt{1-\beta_t}\mathbf{W}_{t-1}, \beta_t \mathbf{I}\right). \end{aligned} \tag{57}$$

For simplicity of expression, we use notations $\mathbf{W}_0$ and $\mathcal{A}_{\mathcal{U}}$ to represent the optimal precoding matrix $\mathbf{W}_0^i$ and the conditional UBS set $\mathcal{A}_{\mathcal{U}}^i$. The specific variance β_t that determines the amount of noise added to $\mathbf{W}_t$ from $\mathbf{W}_{t-1}$ is independent of the conditional UBS set $\mathcal{A}_{\mathcal{U}}$ and remains constant throughout the forward process. Therefore, the distribution for the final T-th noised precoding matrix is expressed by

$$\begin{aligned} q\left(\mathbf{W}_{1:T} | \mathbf{W}_0, \mathcal{A}_{\mathcal{U}}\right) &= \prod_{t=1}^{T} q\left(\mathbf{W}_t | \mathbf{W}_{t-1}, \mathcal{A}_{\mathcal{U}}\right) \\ &= \prod_{t=1}^{T} \mathcal{N}\left(\mathbf{W}_t; \sqrt{1-\beta_t}\mathbf{W}_{t-1}, \beta_t \mathbf{I}\right). \end{aligned} \tag{58}$$

To expedite the forward noise addition process, the diffusion model can directly obtain the noised precoding matrix $\mathbf{W}_t$ for any arbitrary time step t with Gaussian noise $\boldsymbol{\epsilon}_t \sim \mathcal{N}(\mathbf{0}, \mathbf{I})$, which is derived based on the fixed β_t schedule as:

$$\begin{aligned} \mathbf{W}_t &= \sqrt{1-\beta_t}\mathbf{W}_{t-1} + \sqrt{\beta_t}\boldsymbol{\epsilon}_{t-1} \\ &\overset{(5)}{=} \sqrt{\alpha_t}\mathbf{W}_{t-1} + \sqrt{1-\alpha_t}\boldsymbol{\epsilon}_{t-1} \\ &\overset{(6)}{=} \sqrt{\alpha_t\alpha_{t-1}}\mathbf{W}_{t-2} + \sqrt{1-\alpha_t\alpha_{t-1}}\boldsymbol{\epsilon}_{t-2} \\ &\overset{(7)}{=} \sqrt{\bar{\alpha}_t}\mathbf{W}_0 + \sqrt{1-\bar{\alpha}_t}\boldsymbol{\epsilon}_0, \end{aligned} \tag{59}$$

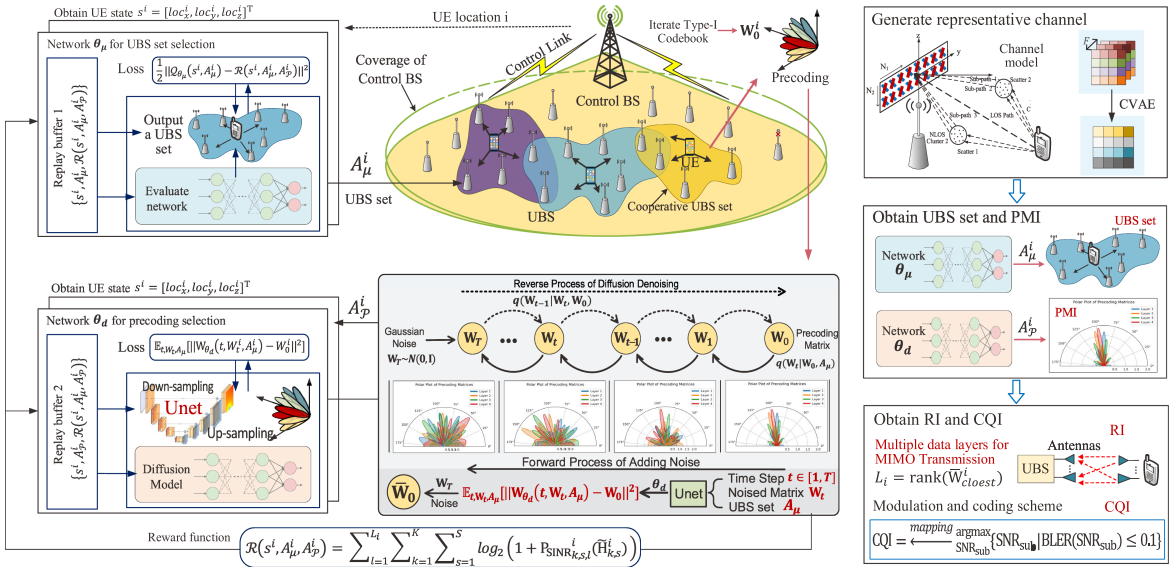

Fig. 3. DRL model for uplink BS set and precoding matrix selection based on diffusion model.

where $\overset{(5)}{=}$ is obtained by setting $\alpha_t := 1 - \beta_t$, and $\overset{(6)}{=}$ is upheld based on the following expression

$$\sqrt{\alpha_t - \alpha_t\alpha_{t-1}}\boldsymbol{\epsilon}_{t-2} + \sqrt{1-\alpha_t}\boldsymbol{\epsilon}_{t-1} = \sqrt{1-\alpha_t\alpha_{t-1}}\boldsymbol{\epsilon}_{t-2}, \tag{60}$$

which stems from the property of summing two Gaussian random variables with variances $\sigma_1 = \sqrt{\alpha_t - \alpha_t\alpha_{t-1}}$ and $\sigma_2 = \sqrt{1-\alpha_t}$ as:

$$\mathcal{N}\left(0, \sigma_1^2\mathbf{I}\right) + \mathcal{N}\left(0, \sigma_2^2\mathbf{I}\right) \sim \mathcal{N}\left(0, \left(\sigma_1^2 + \sigma_2^2\right)\mathbf{I}\right). \tag{61}$$

In addition, $\overset{(7)}{=}$ is attained by iterating the noised precoding matrix $\mathbf{W}_t$ back to the original state $\mathbf{W}_0$ and by setting $\bar{\alpha}_t := \prod_{t'=0}^{t}\alpha_{t'}$. As a result, $\mathbf{W}_t$ is directly obtained for each $t \in [1, T]$ with the formulated distribution

$$\begin{aligned}\mathbf{W}_t \sim q\left(\mathbf{W}_t|\mathbf{W}_0, \mathcal{A}_\mathcal{U}\right) &= q\left(\mathbf{W}_t|\mathbf{W}_0\right) \\ &= \mathcal{N}\left(\mathbf{W}_t; \sqrt{\bar{\alpha}_t}\mathbf{W}_0, \left(1-\bar{\alpha}_t\right)\mathbf{I}\right).\end{aligned} \tag{62}$$

After the forward diffusion process with T-th noise addition steps, $\mathbf{W}_T$ is assumed to follow an isotropic Gaussian distribution. Therefore, the diffusion model performs a reverse process from $\mathbf{W}_T$ to $\mathbf{W}_0$ through sampling a data point out of $\mathcal{N}(\mathbf{0}, \mathbf{I})$ for $\mathbf{W}_T$. With regard to an intermediate transition from $\mathbf{W}_t$ to $\mathbf{W}_{t-1}$, the reverse process can be derived based on the original precoding matrix $\mathbf{W}_0$ as:

$$\begin{aligned}&q\left(\mathbf{W}_{t-1}|\mathbf{W}_t, \mathbf{W}_0\right) \\ &\overset{(8)}{=} q\left(\mathbf{W}_t|\mathbf{W}_{t-1}\right)\frac{q\left(\mathbf{W}_{t-1}|\mathbf{W}_0\right)}{q\left(\mathbf{W}_t|\mathbf{W}_0\right)} \\ &= \mathcal{N}\left(\mathbf{W}_t; \sqrt{\alpha_t}\mathbf{W}_{t-1}, \left(1-\alpha_t\right)\mathbf{I}\right)\cdot \\ &\quad\frac{\mathcal{N}\left(\mathbf{W}_{t-1}; \sqrt{\bar{\alpha}_{t-1}}\mathbf{W}_0, \left(1-\bar{\alpha}_{t-1}\right)\mathbf{I}\right)}{\mathcal{N}\left(\mathbf{W}_t; \sqrt{\bar{\alpha}_t}\mathbf{W}_0, \left(1-\bar{\alpha}_t\right)\mathbf{I}\right)} \\ &= \mathcal{N}\left(\mathbf{W}_{t-1}; \tilde{\boldsymbol{\mu}}_t\left(\mathbf{W}_t, \mathbf{W}_0\right), \tilde{\boldsymbol{\sigma}}_t^2\mathbf{I}\right),\end{aligned} \tag{63}$$

in which $\overset{(8)}{=}$ is obtained based on the Bayes' rule and the mean $\tilde{\boldsymbol{\mu}}_t(\mathbf{W}_t, \mathbf{W}_0)$ and variance $\tilde{\boldsymbol{\sigma}}_t$ values for $\mathbf{W}_{t-1}$ in (63) are calculated by the following results

$$\tilde{\boldsymbol{\mu}}_t\left(\mathbf{W}_t, \mathbf{W}_0\right) = \frac{\sqrt{\bar{\alpha}_{t-1}}\beta_t}{1-\bar{\alpha}_t}\mathbf{W}_0 + \frac{\sqrt{\alpha_t}\left(1-\bar{\alpha}_{t-1}\right)}{1-\bar{\alpha}_t}\mathbf{W}_t, \tag{64}$$

$$\tilde{\boldsymbol{\sigma}}_t^2 = \frac{1-\bar{\alpha}_{t-1}}{1-\bar{\alpha}_t}\left(1-\alpha_t\right). \tag{65}$$

Nonetheless, $q(\mathbf{W}_{t-1}|\mathbf{W}_t, \mathbf{W}_0)$ can not be computed as the reverse process lacks information about $\mathbf{W}_0$. Hence, the diffusion model exploits a parameterized neural network p_{θ_d} to estimate the intermediate reverse transition, which is expressed as follows

$$p_{\theta_d}\left(\mathbf{W}_{t-1}|\mathbf{W}_t\right) = \mathcal{N}\left(\mathbf{W}_{t-1}; \boldsymbol{\mu}_{\theta_d}(t), \boldsymbol{\sigma}_{\theta_d}^2(t)\mathbf{I}\right). \tag{66}$$

The estimated variance $\boldsymbol{\sigma}_{\theta_d}(t)$ can be directly modeled as $\tilde{\boldsymbol{\sigma}}_t$ since $\tilde{\boldsymbol{\sigma}}_t$ possesses a fixed value, denoted by

$$\boldsymbol{\sigma}_{\theta_d}(t) = \tilde{\boldsymbol{\sigma}}_t = \sqrt{\frac{1-\bar{\alpha}_{t-1}}{1-\bar{\alpha}_t}\left(1-\alpha_t\right)}. \tag{67}$$

Subsequently, the network parameter θ_d is optimized by minimizing the KL divergence between $q(\mathbf{W}_{t-1}|\mathbf{W}_t, \mathbf{W}_0)$ and $p_{\theta_d}(\mathbf{W}_{t-1}|\mathbf{W}_t)$ as:

$$\begin{aligned}&\arg\min_{\theta_d} D_{\text{KL}}\left(q\left(\mathbf{W}_{t-1}|\mathbf{W}_t, \mathbf{W}_0\right)\|p_{\theta_d}\left(\mathbf{W}_{t-1}|\mathbf{W}_t\right)\right) \\ &= \mathcal{N}\left(\mathbf{W}_{t-1}; \tilde{\boldsymbol{\mu}}_t, \tilde{\boldsymbol{\sigma}}_t^2\mathbf{I}\right)\|\mathcal{N}\left(\mathbf{W}_{t-1}; \boldsymbol{\mu}_{\theta_d}(t), \tilde{\boldsymbol{\sigma}}_t^2\mathbf{I}\right) \\ &= \frac{1}{2}\left(\left(\boldsymbol{\mu}_{\theta_d}(t) - \tilde{\boldsymbol{\mu}}_t\right)^T\left(\tilde{\boldsymbol{\sigma}}_t^2\right)^{-1}\left(\boldsymbol{\mu}_{\theta_d}(t) - \tilde{\boldsymbol{\mu}}_t\right)\right) \\ &= \frac{1}{2\tilde{\boldsymbol{\sigma}}_t^2}\left\|\boldsymbol{\mu}_{\theta_d}(t) - \tilde{\boldsymbol{\mu}}_t\right\|^2,\end{aligned} \tag{68}$$

in which $\|\boldsymbol{\mu}_{\theta_d}(t) - \tilde{\boldsymbol{\mu}}_t\|^2$ indicates that $\boldsymbol{\mu}_{\theta_d}(t)$ should be approximated as $\tilde{\boldsymbol{\mu}}_t$. A straightforward approach is to design $\boldsymbol{\mu}_{\theta_d}(t)$ in a similar form to $\tilde{\boldsymbol{\mu}}_t$ and allow the network θ_d to approximate the original precoding matrix $\mathbf{W}_0$ based on the

Algorithm 2: Diffusion-Based Precoding Selection.

Input: The optimal precoding matrix $\mathbf{W}_0$ given the cooperative UBS set $\mathcal{A}_{\mathcal{U}}$.
Ouput: An approximated precoding matrix $\bar{\mathbf{W}}$ of $\mathbf{W}_0$.
repeat
  Sample $t \sim \text{Uniform}(\{1, \ldots, T\})$,
  Obtain Gaussian noise $\boldsymbol{\epsilon}_0 \sim \mathcal{N}(\mathbf{0}, \mathbf{I})$,
  Calculate $\mathbf{W}_t = \sqrt{\bar{\alpha}_t}\mathbf{W}_0 + \sqrt{1-\bar{\alpha}_t}\boldsymbol{\epsilon}_0$,
  Update network θ_d based on $\nabla_{\theta_d}\mathbb{E}_{t,\mathbf{W}_t,\mathcal{A}_{\mathcal{U}}}\left[\left\|\mathbf{W}_{\theta_d}(t, \mathbf{W}_t, \mathcal{A}_{\mathcal{U}}) - \mathbf{W}_0\right\|^2\right]$
until *The network θ_d converges*;
Sample $\mathbf{W}_T \sim \mathcal{N}(\mathbf{0}, \mathbf{I})$,
for *time step* $t = T, \cdots, 1$ *(reverse process)* **do**
  if $t > 1$, sample $\mathbf{z} \sim \mathcal{N}(\mathbf{0}, \mathbf{I})$, else $\mathbf{z} = \mathbf{0}$,
  Obtain $\mathbf{W}_{t-1} = \frac{\sqrt{\bar{\alpha}_{t-1}}\beta_t}{1-\bar{\alpha}_t}\mathbf{W}_{\theta_d}(t, \mathbf{W}_t, \mathcal{A}_{\mathcal{U}}) + \frac{\sqrt{\alpha_t}(1-\bar{\alpha}_{t-1})}{1-\bar{\alpha}_t}\mathbf{W}_t, + \frac{1-\bar{\alpha}_{t-1}}{1-\bar{\alpha}_t}(1-\alpha_t)\mathbf{z}$
end
Utilization: Obtain an approximated precoding matrix $\bar{\mathbf{W}}_0$, find the closest precoding matrix $\bar{\mathbf{W}}_{closest}$ to $\bar{\mathbf{W}}_0$ in type-I codebook, and jointly calculate the reward for the DRL framework with UBS set $\mathcal{A}_{\mathcal{U}}$.

given time step t, $\mathbf{W}_t$, and UBS set $\mathcal{A}_{\mathcal{U}}$, formulated by

$$\boldsymbol{\mu}_{\theta_d}(t) = \frac{\sqrt{\bar{\alpha}_{t-1}}\beta_t}{1-\bar{\alpha}_t}\mathbf{W}_{\theta_d}(t, \mathbf{W}_t, \mathcal{A}_{\mathcal{U}}) + \frac{\sqrt{\alpha_t}(1-\bar{\alpha}_{t-1})}{1-\bar{\alpha}_t}\mathbf{W}_t. \tag{69}$$

Therefore, (68) can be transformed into

$$\begin{aligned}&\arg\min_{\theta_d}\frac{1}{2\tilde{\boldsymbol{\sigma}}_t^2}\left\|\boldsymbol{\mu}_{\theta_d}(t) - \tilde{\boldsymbol{\mu}}_t\right\|_2^2,\\ &= \frac{1}{2\tilde{\boldsymbol{\sigma}}_t^2}\frac{\bar{\alpha}_{t-1}\beta_t^2}{(1-\bar{\alpha}_t)^2}\left\|\mathbf{W}_{\theta_d}(t, \mathbf{W}_t, \mathcal{A}_{\mathcal{U}}) - \mathbf{W}_0\right\|^2.\end{aligned} \tag{70}$$

Consequently, the diffusion model leverages the following simpler loss function to update network θ_d

$$\mathcal{L}(\theta_d) := \mathbb{E}_{t,\mathbf{W}_t,\mathcal{A}_{\mathcal{U}}}\left[\left\|\mathbf{W}_{\theta_d}(t, \mathbf{W}_t, \mathcal{A}_{\mathcal{U}}) - \mathbf{W}_0\right\|^2\right]. \tag{71}$$

Based on the network θ_d, the reverse process from Gaussian distributed $\mathbf{W}_T$ to $\mathbf{W}_0$ can be executed and the intermediate transition from $\mathbf{W}_t$ to $\mathbf{W}_{t-1}$ is expressed as:

$$\begin{aligned}\mathbf{W}_{t-1} = &\frac{\sqrt{\bar{\alpha}_{t-1}}\beta_t}{1-\bar{\alpha}_t}\mathbf{W}_{\theta_d}(t, \mathbf{W}_t, \mathcal{A}_{\mathcal{U}}) + \frac{\sqrt{\alpha_t}(1-\bar{\alpha}_{t-1})}{1-\bar{\alpha}_t}\mathbf{W}_t\\ &+ \frac{1-\bar{\alpha}_{t-1}}{1-\bar{\alpha}_t}(1-\alpha_t)\mathbf{z}, \quad \mathbf{z} \sim \mathcal{N}(\mathbf{0}, \mathbf{I}).\end{aligned} \tag{72}$$

In the context of the network structure, a U-net component [49] is utilized within network θ_d to approximate the original precoding matrix $\mathbf{W}_0$. The U-net component comprises down-sampling processes U_{down} and up-sampling processes U_{up} for reconstructing $\mathbf{W}_{\theta_d}(t, \mathbf{W}_t, \mathcal{A}_{\mathcal{U}})$. Both the time step t and the UBS set $\mathcal{A}_{\mathcal{U}}$ are embedded with fully connected (FC) neural networks to match the dimension of $\mathbf{W}_t$, which is denoted by

$$t^{emb} = \text{FC\_embedded}(t), \forall t \in \{0, \ldots, T\}, \tag{73}$$

$$\mathcal{A}_{\mathcal{U}}^{emb} = \text{FC\_embedded}(\mathcal{A}_{\mathcal{U}}), \tag{74}$$

For the j-th down-sampling and up-sampling processes in the U-net, the output of the down-sampling $U_{down}^j(\mathbf{W}_t)$ is first multiplied by the embedded UBS set $\mathcal{A}_{\mathcal{U}}^{emb}$ and then added to the embedded time step t^{emb}. The resulting outcome is concatenated with the output of the j-th up-sampling $U_{up}^j(\mathbf{W}_t)$ and the detailed procedures is formulated in the following

$$U_{up}^{j+1} = \left(\mathcal{A}_{\mathcal{U}}^{emb} \times U_{down}^j(\mathbf{W}_t) + t^{emb}\right) \oplus U_{up}^j(\mathbf{W}_t). \tag{75}$$

With the reconstructed $\mathbf{W}_{\theta_d}(t, \mathbf{W}_t, \mathcal{A}_{\mathcal{U}})$ for each time step t and the total T-th diffusion reverse process, we can obtain an approximated precoding matrix $\bar{\mathbf{W}}_0$ of the original $\mathbf{W}_0$. Euclidean distance is then used to select a precoding matrix from the type-I codebook that is closest to $\bar{\mathbf{W}}_0$, indicated by $\bar{\mathbf{W}}_{closest}$. $\bar{\mathbf{W}}_{closest}$ together with the UBS set $\mathcal{A}_{\mathcal{U}}$ will jointly decide the reward in (54) for the proposed DRL framework. The detailed procedures of the diffusion model enabled precoding selection is described in Algorithm 2.

Algorithm 3: Cooperative Uplink Feedback-Free Mechanism.

Input: Original N_f subframe channels $\{\mathbf{H}_{k,s,f}^i\}_{f=1}^F$.
Ouput: Time-invariant PMI, RI, CQI, and UBS set.
Obtain a representative channel $\widetilde{\mathbf{H}}_{k,s}^i$ for $\{\mathbf{H}_{k,s,f}^i\}_{f=1}^F$ based on **Algorithm** 1 to solve problem (29).
repeat
  Obtain UE state $\mathbf{s}^i = \left[loc_x^i,\ loc_y^i,\ loc_z^i\right]^{\mathrm{T}}$, $\forall i \in \mathcal{I}$,
  Select an action of UBS set $\mathcal{A}_{\mathcal{U}}^i$ based on the output $\mathcal{Q}$-values $\mathcal{Q}_{\theta_{\mathcal{U}}}(\mathbf{s}^i)$ of the network $\theta_{\mathcal{U}}$,
  Iterate the type-I codebook to obtain optimal $\bar{\mathbf{W}}_0^i$ given the UBS set $\mathcal{A}_{\mathcal{U}}^i$,
  Select the precoding matrix $\bar{\mathbf{W}}_{closest}^i$ that is closest to $\bar{\mathbf{W}}_0^i$ using **Algorithm** 2,
  Calculate reward $\mathcal{R}(\mathbf{s}^i, \mathcal{A}_{\mathcal{U}}^i, \mathcal{A}_{\mathcal{P}}^i)$ based on Eq. (54),
  Update network $\theta_{\mathcal{U}}$ based on $\nabla_{\theta_{\mathcal{U}}}\mathcal{L}(\theta_{\mathcal{U}}) = \frac{1}{2}\left\|\mathcal{Q}_{\theta_{\mathcal{U}}}(\mathbf{s}^i, \mathcal{A}_{\mathcal{U}}^i) - \mathcal{R}(\mathbf{s}^i, \mathcal{A}_{\mathcal{U}}^i; \mathcal{A}_{\mathcal{P}}^i)\right\|^2$,
  Update network θ_d based on $\nabla_{\theta_d}\mathbb{E}_{t,\mathbf{W}_t^i,\mathcal{A}_{\mathcal{U}}^i}\left[\left\|\mathbf{W}_{\theta_d}(t, \mathbf{W}_t^i; \mathcal{A}_{\mathcal{U}}^i) - \mathbf{W}_0^i\right\|^2\right]$.
until *The networks $\theta_{\mathcal{U}}$ and θ_d converges*;
Calculate data stream number $L_i = \text{rank}\left(\bar{\mathbf{W}}_{closest}^i\right)$,
Calculate a CQI value based on Eqs. (23) - (25).
Utilization: Use the obtained time-invariant PMI, RI, CQI, and cooperative UBS set for cooperative uplink feedback-free transmission across all time periods.

D. Overall Cooperative Uplink Feedback-Free Mechanism

The proposed cooperative uplink feedback-free mechanism involves the determination of time-invariant transmission parameters including PMI, RI, CQI, and cooperative UBS set for each UE. Problem (27) is formulated to obtain an effective

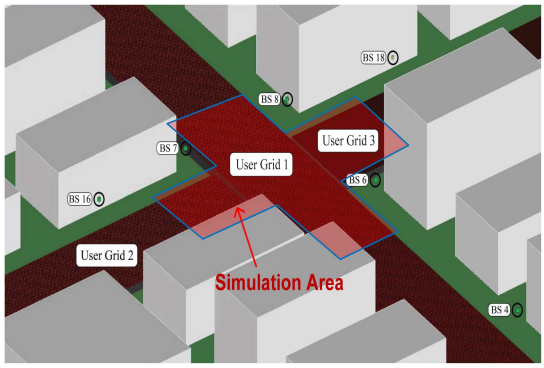

Fig. 4. DeepMIMO Outdoor 1 (O1) scenario.

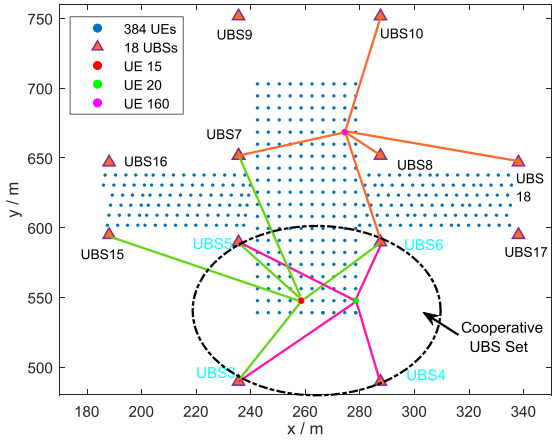

Fig. 5. The position coordinates of 2 DBS and 1138 UE.

PMI, RI, and cooperative UBS set over F stochastic subframe channels $\{\mathbf{H}^i_{k,s,f}\}_{f=1}^{F}$. Utilizing Algorithm 1, CAE generates a representative channel $\widetilde{\mathbf{H}}^i_{k,s}$ for subcarrier k, OFDM symbol s, and UE i, which eliminates the stochastic property of the wireless channel and transforms problem (27) into problem (29). In the proposed diffusion model based DRL framework, the network $\theta_{\mathcal{U}}$ will output a UBS set $\mathcal{A}^i_{\mathcal{U}}$ and the diffusion model will select the precoding matrix $\bar{\mathbf{W}}^i_{cloest}$ from type-I codebook based on Algorithm 2 to jointly calculate the reward for UE i. Furthermore, RI for the number of data stream L_i is obtained as rank$(\bar{\mathbf{W}}^i_{cloest})$. After the DRL training converges, the attained PMI, RI, and UBS set of each UE will be taken into the calculation of a CQI value based on Eqs. (23)–(25). The overall procedure to obtain a time-invariant PMI, RI, CQI, and cooperative UBS set for the uplink feedback-free transmission is given in Algorithm 3.

For the proposed DRL framework, the UBS selection network $\theta_{\mathcal{U}}$ and the diffusion model-based precoding network θ_d are updated by taking gradient decent over $\mathcal{L}(\theta_{\mathcal{U}}) = \frac{1}{2}\|\mathcal{Q}_{\theta_{\mathcal{U}}}(\mathbf{s}^i, \mathcal{A}^i_{\mathcal{U}}) - \mathcal{R}(\mathbf{s}^i, \mathcal{A}^i_{\mathcal{U}}; \mathcal{A}^i_{\mathcal{P}})\|^2$ and $\mathbb{E}_{t,\mathbf{W}^i_t,\mathcal{A}^i_{\mathcal{U}}}[\|\mathbf{W}_{\theta_d}(t, \mathbf{W}^i_t; \mathcal{A}^i_{\mathcal{U}}) - \mathbf{W}^i_0\|^2]$, respectively. The overall DRL framework alternately updates the network $\theta_{\mathcal{U}}$ and the network θ_d. Specifically, $\theta_{\mathcal{U}}$ is updated while fixing θ_d, and vice versa. This alternating procedure follows a standard bi-level optimization mechanism, where each subnetwork is trained using SGD approach. Consequently, the DRL training process is stable and can converge to a stationary solution [50]. In each training iteration, network $\theta_{\mathcal{U}}$ requires evaluating all feasible cooperative UBS sets, leading to a per-iteration complexity of $\mathcal{O}(|\mathcal{A}_U|\zeta_U)$, where ζ_U is the forward cost of $\theta_{\mathcal{U}}$. The diffusion model requiring one U-Net forward computation denoted as ζ_d for T denoising steps, resulting in a complexity of $\mathcal{O}(T\zeta_d)$. Additionally, the search for the closest precoding matrix in the Type-I codebook costs $\mathcal{O}(|\mathcal{P}|d_{\mathcal{P}})$ with $d_{\mathcal{P}}$ denoting the precoding dimension. Consequently, the overall computational complexity of the proposed DRL algorithm with T_D training steps is expressed as $\mathcal{O}(T_D(|\mathcal{A}_U|\zeta_U + T\zeta_d + |\mathcal{P}|d_{\mathcal{P}}))$.

V. Simulation Results

This section conducts extensive simulations utilizing the Vienna 5G Link-Level Simulator [26] to validate the performance of cooperative multi-BS reception. As illustrated in Fig. 4, the Outdoor 1 (O1) [51] scenario from DeepMIMO is implemented as the simulation environment. The simulation setup includes all 18 BSs of the DeepMIMO O1 scenario and 384 UE positions in the red area of Fig. 4, the position coordinates of which are shown in Fig. 5. Each UE is equipped with a 2×1 dual-polarized transmitting antenna, with a total antenna count of $N_{\text{tx}} = 4$, while the UBS is equipped with a 4×1 dual-polarized receiving antenna, with a total antenna count of $N_{\text{rx}} = 8$ [48]. The $3D$ channel model is simulated based on DeepMIMO's ray tracing technology, operating at a center frequency of 3.5 GHz [52] with 100 time-varying subframe channels. One transmission subframe consists of 72 subcarriers and 14 OFDM symbols,which have a duration of 1 ms [53]. The total duration for 100 transmission subframes is 100ms. Since the UE has $N_{\text{tx}} = 4$ transmitting antennas, it supports a maximum of 4 data streams for spacial transmission [42]. The MCS, precoding, MIMO streams, and cooperative BS set are simulated based on complete physical layer module of the Vienna 5G Link-Level Simulator, allowing for measurement of the BER and the data volume successfully transmitted by the UE in megabits per second (Mbit/s). The relationship between the UE throughput and the BER is expressed as $Throughput = (1 - BER) \times transmitted\,bits\,per\,second$. The detailed settings of the simulation parameters are provided in Table I.

TABLE I
Parameters Settings

Parameter	Value	Parameter	Value
Number of UE positions	384	Number of UBSs	18
Number of UE antenna	4	Number of UBS antenna	8
UE dual-polarization	2×1	UBS dual-polarization	4×1
Number of subcarriers	72	Number of OFDM symbols	14
Center frequency	3.5 GHz	Simulation subframes	100
Number of data streams	1 - 4	Subframe duration	1 ms
Modulation scheme	QPSK - 64QAM	Simulation duration	100 ms
Coding scheme	$LDPC$	Number of precoding matrix	128

A. Evaluation of Diffusion Model-Based DRL Framework

We first test the performance of the diffusion model-based DRL framework on cooperative BS and precoding selection for

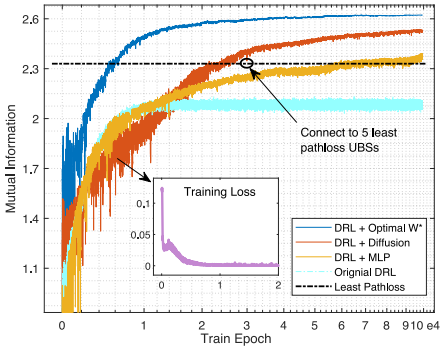

Fig. 6. The training process of DRL.

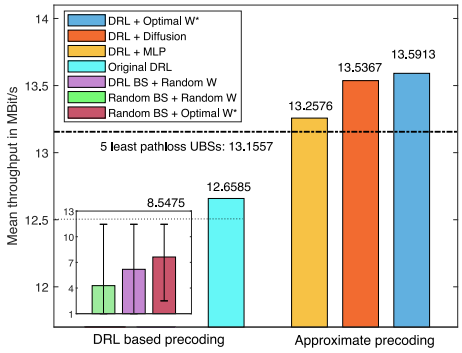

Fig. 7. Average throughput of 384 UEs.

multi-BS reception. Fig. 6 illustrates the training process of various DRL training schemes, which select no more than $N_b = 5$ out of 18 UBSs and one precoding matrix from 128 options in the type-I codebook. The original DRL framework independently outputs the actions of $\mathcal{A}_{\mathcal{U}}^i$ and $\mathcal{A}_{\mathcal{P}}^i$ for the cooperative BS set and precoding matrix, resulting in the worst training performance due to the lack of expert knowledge regarding the optimal precoding matrix. Replacing the precoding network with MLP layers to approximate the optimal precoding significantly improves the training mutual information for multi-BS reception. Meanwhile, in the early training stage, the diffusion-based DRL approach performs worse than the MLP layers. When the diffusion model converges, the training performance approaches 97% of the performance achieved by the DRL training using the optimal precoding matrices, validating the effectiveness of the diffusion model in approximate complex data distributions. Additionally, Fig. 6 demonstrates the mutual information of 5 least path loss UBSs with optimal precoding matrices. The simulation results indicate that the diffusion based-DRL outperforms this benchmark, due to the fact that the wireless channel is influenced not only by large-scale fading but also by small-scale fading.

Fig. 5 provides an illustration of the cooperative BS set for UE 15, 20, and 160, respectively, based on the training results of the proposed diffusion-based DRL approach. In Fig. 7, the proposed approach achieves an average throughput of 13.54 Mbit/s, outperforming the MLP-based variant (13.26 Mbit/s), the minimum 5-UBS path-loss benchmark (13.16 Mbit/s), and the original DRL framework without precoding approximation (12.66 Mbit/s). Furthermore, the throughput of the diffusion-based DRL algorithm is only slightly lower than that of the DRL scheme with optimal precoding (13.59 Mbit/s), demonstrating that the proposed method can effectively approximate the optimal solution with marginal performance loss. In addition, two benchmarks, i.e., DRL-based BS selection with random precoding and random BS selection with random precoding, achieve notably lower throughput. Even when adopting the optimal precoding matrix, the random BS selection scheme attains only 8.55Mbit/s, which is considerably lower than the proposed diffusion-based DRL method. These results demonstrate that the proposed DRL framework not only optimizes the precoding weights but also effectively learns the BS–UE association strategy.

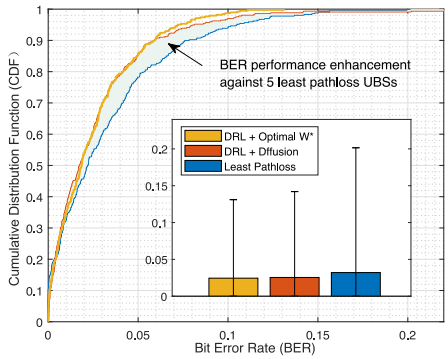

Fig. 8. CDF plot for 384 UEs' BER.

Fig. 8 presents the cumulative distribution function (CDF) and average values of the bit error rate (BER) for different DRL algorithms based on the Vienna Link-Level Simulator. The DRL training using optimal precoding matrices has the lowest BER, followed by the diffusion model-based DRL approach, while the fixed connection of the 5 UBSs with the minimum path loss possesses a higher BER compared to the former two schemes. The simulation results are consistent with the training results in Fig. 6 and the throughput results in Fig. 7. In addition, the gray area in Fig. 8 illustrates the BER performance gain of the diffusion-based DRL approach compared to the benchmark of 5 minimum path loss UBSs.

B. Evaluation of Representative Channels Generated by CVAE

This subsection tests the performance of the representative channels generated by the CVAE in comparison to other subframe channels. Fig. 9 presents the throughput performance of multi-BS transmission based on the representative channels when connecting to 5 UBSs with the minimum path loss (not considering the cooperative BS set). To provide a clearer comparison of the throughput performance, the first 40 UEs are selected to demonstrate the average throughput across 100 subframes using the transmission parameters calculated with both CVAE-generated representative channels, subframe channels 1–5, and a conditional generative adversarial network (CGAN) baseline. The CGAN generates representative channels using a generator trained with the same subframe channel as the

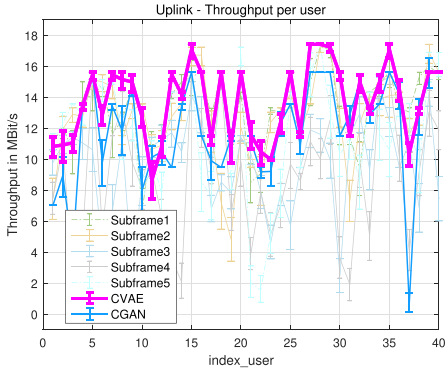

Fig. 9. Throughput of 1-40 UEs under CVAE, CGAN, and subframe channels.

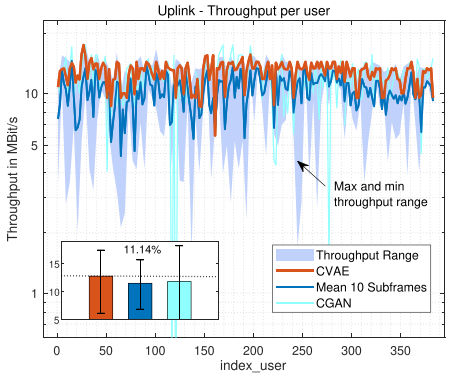

Fig. 10. Throughput of 384 UEs under CVAE, CGAN, and subframe channels.

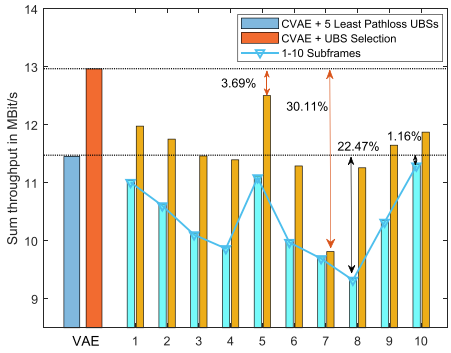

Fig. 11. Throughput comparison between CVAE and subframe channels.

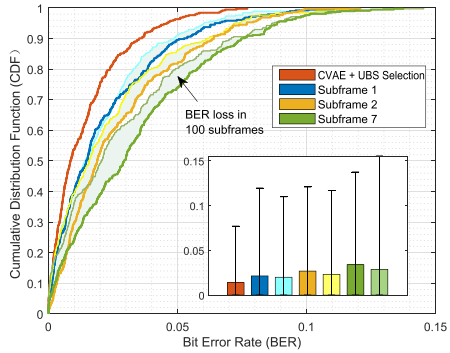

Fig. 12. The CDF and average BER under CSI feedback-free transmission.

conditional input and random noise vectors as the stochastic source, aiming to learn the mapping between conditional features and representative channels. It can be observed that the throughput performance achieved by the CVAE surpasses that of both the subframe channels 1–5 and the CGAN-based representative channels. Moreover, the CVAE achieves the maximum throughput of the 5 subframe channels at most UE positions, indicating that the CVAE-generated representative channels can better capture dynamic variations and adapt to time-varying wireless channel environments.

Fig. 10 illustrates the multi-BS reception throughput of all 384 UEs based on the PMI, RI, CQI, and cooperative BS set calculated with the CVAE-generated representative channels, 10 different subframe channels, and the CGAN baseline. The light blue area in the figure represents the throughput fluctuation range with maximum and minimum values for the 10 different subframes at each user location. Compared with both the CGAN baseline and the 10 subframe channels, the proposed CVAE achieves the highest throughput at most of the 384 UE positions, and the average throughput is improved by 11.14% over the mean value of the 10 subframes. In addition, the CVAE consistently exhibits smaller throughput fluctuation compared with the CGAN-based method, demonstrating more stable reconstruction and better adaptation to dynamic channel variations. This improvement arises due to the reason that CVAE can generate multiple latent variables and select the one whose statistical characteristics (mean and variance) are closest to the encoded latent distribution for channel generation, rather than directly producing samples from random noise as in GANs (see (44)).

Fig. 11 details the average throughput obtained by the 10 subframe channels. For the scenario where 5 UBSs with the minimum path loss are connected, the representative channels based on the CVAE can improve throughput performance by at least 1.16% compared to the 10 subframe channels and achieve a maximum throughput gain of 22.47%. For the scenario of selecting the cooperative BS set, the representative channels can improve throughput by at least 3.69% and realize a maximum throughput gain of 30.11%.

Fig. 12 illustrates the CDF and the average values of BER for the CVAE-generated representative channel and subframe channels 1, 2, and 7. The green areas in the figure represent the BER loss during the 100 subframe transmission process, using the PMI, RI, CQI, and cooperative BS set calculated with subframe channels. Additionally, it can be seen that using the transmission parameters calculated with the representative channel achieves the lowest transmission BER. The simulation result further validates the effectiveness of time-domain representative channels generated by GAI methods, providing a feasible approach for implementing the CSI feedback-free mechanism in uplink multi-BS reception.

C. Evaluation of CSI Feedback-Free Transmission

This subsection tests the performance of cooperative multi-BS reception based on the CSI feedback-free transmission mechanism and real-time CSI feedback mechanism across 100

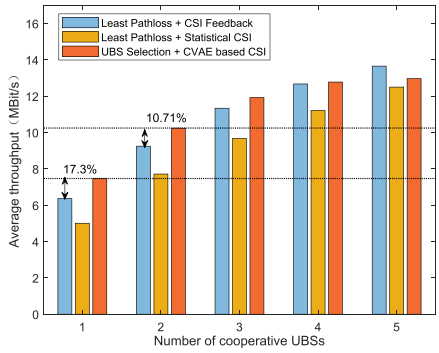

Fig. 13. The UE throughput under different transmission mechanisms.

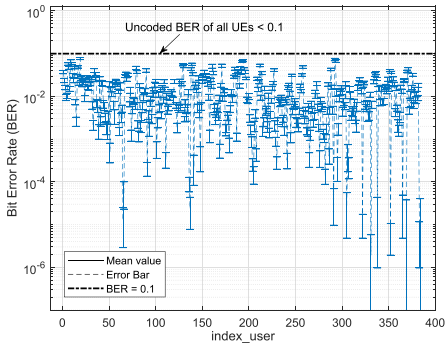

Fig. 14. The uncoded BER of 384 UEs under CSI feedback-free transmission.

subframes. The CSI feedback-free transmission mechanism employs time-invariant PMI, RI, CQI, and cooperative BS set based on the CVAE-generated representative channels. For the real-time CSI feedback mechanism, the PMI, RI, and CQI are obtained using real-time channel matrices. However, since it is impractical to calculate the cooperative BS set within 1 ms subframe duration, the real-time CSI feedback mechanism consistently connects to the BSs with the minimum path loss during the 100 subframe transmission process.

Fig. 13 presents the average throughput performance of 384 UEs when connecting 1 to 5 UBSs for across 100 subframes. Since the direct use of statistical parameters does not adequately adapt to the dynamically changing channels, this method results in the lowest average throughput. Besides, when connecting to 1 UBS, the feedback-free throughput using the representative channels outperforms the average throughput based on the real-time CSI feedback mechanism by 17.3%. This result arises from the connection to the UBS with with the minimum path loss in CSI feedback mechanism, without considering the effects of small-scale fading and failing to achieve optimal performance. Furthermore, Fig. 14 illustrates the BER performance during the feedback-free transmission across 100 subframes for 384 UEs. It can be observed that for the CSI feedback-free transmission based on representative channels, the majority of UEs have a uncoded BER distribution between 10^{-2} and 10^{-4}, meeting the basic requirements for BER in current wireless communication systems.

VI. Conclusion

In this paper, we have investigated a feedback-free uplink joint reception mechanism within the FD-RAN architecture, aiming to mitigate the substantial communication and computational overhead caused by real-time CSI feedback. Given the temporal dynamics of wireless channels, we have proposed a CVAE-based GenAI model to generate time-domain representative channels from historical CSI distributions. Furthermore, in the spatial domain, we have developed a diffusion-enhanced DRL framework to jointly determine the cooperative BS sets, precoding matrices, MIMO streams, and MCS parameters, providing a scalable and efficient solution to physical layer optimization. Simulation results based on a comprehensive link-level simulator demonstrate that the proposed feedback-free scheme achieves a 17.3% improvement in spectral efficiency compared to conventional CSI-based designs. In future work, we will further explore innovative AI techniques, such as large foundation models, to enhance FD-RAN feedback-free transmission and facilitate its practical deployment in sixth-generation wireless networks.

References

[1] S. Elhoushy, M. Ibrahim, and W. Hamouda, "Cell-free massive MIMO: A survey," *IEEE Commun. Surv. Tuts.*, vol. 24, no. 1, pp. 492–523, 1st Quart., 2021.
[2] J. Zhao et al., "Fully-decoupled radio access networks: A resilient uplink base stations cooperative reception framework," *IEEE Trans. Wireless Commun.*, vol. 22, no. 8, pp. 5096–5110, Aug. 2023.
[3] G. Femenias and F. Riera-Palou, "Mobile edge computing aided cell-free massive MIMO networks," *IEEE Trans. Mobile Comput.*, vol. 23, no. 2, pp. 1246–1261, Feb. 2024.
[4] 3GPP, "NR; user equipment (UE) radio access capabilities," 3rd Generation Partnership Project (3GPP), Technical Specification (TS) 38.306, Aug. 2022, v15.17.0.
[5] H. A. Ammar et al., "User-centric cell-free massive MIMO networks: A survey of opportunities, challenges and solutions," *IEEE Commun. Surv. Tuts.*, vol. 24, no. 1, pp. 611–652, 1st Quart., 2021.
[6] R. Chopra, C. R. Murthy, and A. K. Papazafeiropoulos, "Uplink performance analysis of cell-free mMIMO systems under channel aging," *IEEE Commun. Lett.*, vol. 25, no. 7, pp. 2206–2210, Jul. 2021.
[7] Y. Xu et al., "Federated learning over fully-decoupled RAN architecture for two-tier computing acceleration," *IEEE J. Sel. Areas Commun.*, vol. 41, no. 3, pp. 789–801, Mar. 2023.
[8] X. Zhang, X. Qin, Y. Wang, Y. Xu, H. Zhou, and W. Zhuang, "Robust downlink data transmission in leo satellite–terrestrial networks: A rate-splitting multiple access approach," *IEEE Internet Things J.*, vol. 12, no. 14, pp. 27364–27378, Jul. 2025.
[9] S. Chen, J. Zhang, E. Björnson, Ö. T. Demir, and B. Ai, "Energy-efficient cell-free massive MIMO through sparse large-scale fading processing," *IEEE Trans. Wireless Commun.*, vol. 22, no. 12, pp. 9374–9389, Dec. 2023.
[10] G. Femenias and F. Riera-Palou, "From cells to freedom: 6G's evolutionary shift with cell-free massive MIMO," *IEEE Trans. Mobile Comput.*, vol. 24, no. 2, pp. 812–829, Feb. 2025.
[11] Q. Yu et al., "A fully-decoupled ran architecture for 6G inspired by neurotransmission," *J. Commun. Inf. Netw.*, vol. 4, no. 4, pp. 15–23, 2019.
[12] B. Qian et al., "Enabling fully-decoupled radio access with elastic resource allocation," *IEEE Trans. Cognit. Commun. Netw.*, vol. 9, no. 4, pp. 1025–1040, Aug. 2023.
[13] T. Zhang et al., "Toward handover-free mobility management in FD-RAN: Architecture, challenges, and solutions," *IEEE Netw.*, vol. 38, no. 6, pp. 433–442, Nov. 2024.
[14] N. Kim, I. P. Roberts, and J. Park, "Splitting messages in the dark-rate-splitting multiple access for FDD massive MIMO without CSI feedback," *IEEE Trans. Wireless Commun.*, vol. 24, no. 4, pp. 3320–3332, Apr. 2025.
[15] K. Yu et al., "Fully-decoupled radio access networks: A flexible downlink multi-connectivity and dynamic resource cooperation framework," *IEEE Trans. Wireless Commun.*, vol. 22, no. 6, pp. 4202–4214, Jun. 2023.

[16] J. Liu, J. Chen, Z. Liu, and H. Zhou, "Enabling feedback-free MIMO transmission for FD-RAN: A data-driven approach," *IEEE Trans. Mobile Comput.*, vol. 24, no. 3, pp. 2437–2454, Mar. 2025.
[17] Z. Lyu, M. Xiao, J. Xu, M. Skoglund, and M. Di Renzo, "The larger the merrier? Efficient large AI model inference in wireless edge networks," 2025, *arXiv:2505.09214*.
[18] M. Elamassie and M. Uysal, "Feedback-free adaptive modulation selection algorithm for FSO systems," *IEEE Wireless Commun. Lett.*, vol. 10, no. 9, pp. 1964–1968, Sep. 2021.
[19] Y. Xu et al., "Decentralization of generative AI via mixture of experts for wireless networks: A comprehensive survey," 2025, *arXiv:2504.19660*.
[20] M. Sheraz et al., "A comprehensive survey on GenAI-enabled 6G: Technologies, challenges, and future research avenues," *IEEE Open J. Commun. Soc.*, vol. 6, pp. 4563–4590, 2025.
[21] J. Xue et al., "Cooperative deep reinforcement learning enabled power allocation for packet duplication URLLC in multi-connectivity vehicular networks," *IEEE Trans. Mobile Comput.*, vol. 23, no. 8, pp. 8143–8157, Aug. 2024.
[22] Y. Xu et al., "Fully-decoupled ran for feedback-free multi-base station transmission in MIMO-OFDM system," *IEEE J. Sel. Areas Commun.*, vol. 43, no. 3, pp. 780–794, Mar. 2025.
[23] Z. Liu et al., "Leveraging self-supervised learning for MIMO-OFDM channel representation and generation," 2024, *arXiv:2407.07702*.
[24] Y. Xu et al., "Leveraging multiagent learning for automated vehicles scheduling at nonsignalized intersections," *IEEE Internet Things J.*, vol. 8, no. 14, pp. 11427–11439, Jul. 2021.
[25] L. Bai, J. Xu, J. Wang, R. Han, and J. Choi, "Efficient hybrid transmission for cell-free systems via NOMA and multiuser diversity," *IEEE Trans. Mobile Comput.*, vol. 24, no. 4, pp. 3359–3371, Apr. 2025.
[26] S. Pratschner et al., "Versatile mobile communications simulation: The vienna 5G link level simulator," *EURASIP J. Wireless Commun. Netw.*, vol. 2018, no. 1, 2018, Art. no. 226.
[27] F. Z. Morais et al., "When SDN meets C-RAN: A survey exploring multi-point coordination, interference, and performance," *J. Netw. Comput. Appl.*, vol. 162, 2020, Art. no. 102655.
[28] H. Q. Ngo et al., "Cell-free massive MIMO versus small cells," *IEEE Trans. Wireless Commun.*, vol. 16, no. 3, pp. 1834–1850, Mar. 2017.
[29] E. Björnson et al., "Massive MIMO networks: Spectral, energy, and hardware efficiency," *Foundations Trends Signal Process.*, vol. 11, no. 3-4, pp. 154–655, 2017.
[30] E. Björnson and L. Sanguinetti, "Scalable cell-free massive MIMO systems," *IEEE Trans. Commun.*, vol. 68, no. 7, pp. 4247–4261, Jul. 2020.
[31] 3GPP, "Evolved universal terrestrial radio access (E-UTRA); physical layer procedures," 3rd Generation Partnership Project (3GPP), Technical specification (TS) 36.213, Jun. 2022, version 17.2.0.
[32] J. Shi et al., "Learning to compute ergodic rate for multi-cell scheduling in massive MIMO," *IEEE Trans. Wireless Commun.*, vol. 20, no. 2, pp. 785–797, Feb. 2021.
[33] Z. Wang, J. Zhang, H. Q. Ngo, B. Ai, and M. Debbah, "Uplink precoding design for cell-free massive MIMO with iteratively weighted MMSE," *IEEE Trans. Commun.*, vol. 71, no. 3, pp. 1646–1664, Mar. 2023.
[34] W. Jiang and H. D. Schotten, "Opportunistic ap selection in cell-free massive MIMO-OFDM systems," in *Proc. IEEE Veh. Technol. Conf.*, 2022, pp. 1–5.
[35] C. He, Y. Lu, B. Ai, O. A. Dobre, Z. Ding, and D. Niyato, "ICGNN: Graph neural network enabled scalable beamforming for MISO interference channels," *IEEE Trans. Mobile Comput.*, vol. 24, no. 10, pp. 10778–10791, Oct. 2025.
[36] Z. Jiwei, C. Jiacheng, S. Zeyu, S. Yuhang, Z. Haibo, and X. S. Shen, "Channel-feedback-free transmission for downlink FD-RAN: A radio map based complex-valued precoding network approach," *China Commun.*, vol. 21, no. 4, pp. 10–22, 2024.
[37] X. Zhang, X. Qin, Z. Zhang, L. X. Cai, H. Zhou, and W. Zhuang, "RIS-aided MIMO downlink transmission for ultradense LEO satellite-terrestrial networks," *IEEE Internet Things J.*, vol. 12, no. 11, pp. 15304–15318, Jun. 2025.
[38] W. Wang, B. Yang, and W. Zhang, "Deep learning-based radio map for MIMO-OFDM downlink precoding," *J. Commun. Inf. Netw.*, vol. 8, no. 3, pp. 203–211, 2023.
[39] J. Liu, J. Chen, Z. Liu, Y. Xu, J. Kang, and H. Zhou, "A variational autoencoder enabled feedback-free MIMO transmission approach for FD-RAN," in *Proc. IEEE Glob. Commun. Conf.*, 2024, pp. 469–474.
[40] A. Alkhateeb, "DeepMIMO: A generic deep learning dataset for millimeter wave and massive MIMO applications," 2019, *arXiv:1902.06435*.
[41] D. Tse and P. Viswanath, *Fundamentals of Wireless Communication*. Cambridge, U.K.: Cambridge Univ. Press, 2005.
[42] R. W. Heath Jr and A. Lozano, *Foundations of MIMO Communication*. Cambridge, U.K.: Cambridge Univ. Press, 2018.
[43] S. Schwarz, C. Mehlführer, and M. Rupp, "Calculation of the spatial preprocessing and link adaption feedback for 3GPP UMTS/LTE," in *Proc. Wireless Adv. 2010*, 2010, pp. 1–6.
[44] K. Shen and W. Yu, "Fractional programming for communication systems—Part I: Power control and beamforming," *IEEE Trans. Signal Process.*, vol. 66, no. 10, pp. 2616–2630, May 2018.
[45] Z.-Q. Luo and S. Zhang, "Dynamic spectrum management: Complexity and duality," *IEEE J. Sel. Topics Signal Process.*, vol. 2, no. 1, pp. 57–73, Feb. 2008.
[46] D. P. Kingma and M. Welling, "Auto-encoding variational bayes," 2013, *arXiv:1312.6114*.
[47] S. Ghadimi and G. Lan, "Stochastic first-and zeroth-order methods for nonconvex stochastic programming," *SIAM J. Optim.*, vol. 23, no. 4, pp. 2341–2368, 2013.
[48] 3GPP, "NR; physical layer procedures for data," Technical specification (TS) 38.214, Jan. 2024, v18.1.0.
[49] J. Ho, A. Jain, and P. Abbeel, "Denoising diffusion probabilistic models," in *Proc. Adv. Neural Inf. Process. Syst.*, 2020, pp. 6840–6851.
[50] P. Tseng, "Convergence of a block coordinate descent method for nondifferentiable minimization," *J. Optim. Theory Appl.*, vol. 109, no. 3, pp. 475–494, 2001.
[51] A. Alkhateeb, "DeepMIMO: A generic deep learning dataset for millimeter wave and massive MIMO applications," in *Proc. Inf. Theory Appl. Workshop (ITA)*, San Diego, CA, Feb. 2019, pp. 1–8.
[52] 3GPP, "Study on channel model for frequencies from 0.5 to 100 GHz," Technical report (TR) 38.901, Apr. 2024, v18.0.0.
[53] 3GPP, "NR; physical channels and modulation," Technical specification (TS) 38.211, Mar. 2024, v18.2.0.

Haibo Zhou (Fellow, IEEE) received the PhD degree in information and communication engineering from Shanghai Jiao Tong University, Shanghai, China, in 2014. From 2014 to 2017, he was a postdoctoral fellow with the Broadband Communications Research Group, Department of Electrical and Computer Engineering, University of Waterloo. He is currently a full professor with the School of Electronic Science and Engineering, Nanjing University, Nanjing, China. He was a recipient of the 2019 IEEE ComSoc Asia–Pacific Outstanding Young Researcher Award, 2023 IEEE ComSoc WTC Outstanding Young Researcher Award, 2023-2024 IEEE ComSoc Distinguished Lecturer, and 2023-2025 IEEE VTS Distinguished Lecturer. He served as Track/Symposium Co-Chair for IEEE/CIC ICCC 2019, IEEE VTC-Fall 2020, IEEE VTC-Fall 2021, WCSP 2022, IEEE GLOBECOM 2022, IEEE ICC 2024, IEEE GLOBECOM 2024. He is currently an associate editor of *IEEE Transactions on Wireless Communications*, *IEEE Internet of Things Journal*, *IEEE Network Magazine*, and *Journal of Communications and Information Networks*. His research interests include resource management and protocol design in B5G/6G networks, vehicular ad hoc networks, and space-air-ground integrated networks.

Yunting Xu (Member, IEEE) received the PhD degree from Nanjing University, in 2024. He is currently a research fellow with the School of Computer Science and Engineering, Nanyang Technological University, Singapore. He mainly focuses on the artificial intelligence and networking optimization in the field of emerging wireless networks.

Tianqi Zhang (Member, IEEE) received the BS degree in electronical information science and technology from Nanjing University, Nanjing, China, in 2021, where he is currently working toward the PhD degree in information and communication engineering with Nanjing University. His current research interests include dynamic resource scheduling, mobility management, and machine learning in the field of emerging wireless networks.

Xin Zhang (Member, IEEE) received the BS degree from the University of Electronic Science and Technology of China, in 2020, and the PhD degree from Nanjing University, in 2025. She is currently a postdoctoral fellow with the School of Electronic Science and Engineering, Nanjing University, Nanjing, China. Her research interests include space-air-ground integrated networks, resource allocation, and convex optimization theory.

Jiacheng Chen (Member, IEEE) received the PhD degree in information and communications engineering from Shanghai Jiao Tong University, Shanghai, China, in 2018. From 2015 to 2016, he was a visiting scholar with BBCR group, University of Waterloo, Canada. Currently, he is an assistant researcher with Pengcheng Laboratory, Shenzhen, China. His research interests include fully-decoupled radio access network technologies. He has served as the guest editor for IEEE IoTJ, and the Workshop Co-chair for IEEE/CIC ICCC from 2021 to 2024. He was the recipient of *Journal of Communications and Information Networks (JCIN)* Best Paper Award in 2016, and the Chinese Institute of Electronics (CIE) Outstanding Scientific Paper in the Field of Electronic Information in 2020.

Xuemin Shen (Fellow, IEEE) received the PhD degree in electrical engineering from Rutgers University, New Brunswick, NJ, USA, in 1990. He is a university professor with the Department of Electrical and Computer Engineering, University of Waterloo, Canada. His research focuses on network resource management, wireless network security, Internet of Things, AI for networks, and vehicular networks. He is a registered professional engineer of Ontario, Canada, an Engineering Institute of Canada Fellow, a Canadian Academy of Engineering Fellow, a Royal Society of Canada Fellow, a Chinese Academy of Engineering Foreign Member, an International Fellow of the Engineering Academy of Japan, and a Distinguished Lecturer of the IEEE Vehicular Technology Society and Communications Society. He received "West Lake Friendship Award" from Zhejiang Province in 2023, President's Excellence in Research from the University of Waterloo in 2022, the Canadian Award for Telecommunications Research from the Canadian Society of Information Theory (CSIT) in 2021, the R.A. Fessenden Award in 2019 from IEEE, Canada, Award of Merit from the Federation of Chinese Canadian Professionals (Ontario) in 2019, James Evans Avant Garde Award in 2018 from the IEEE Vehicular Technology Society, Joseph LoCicero Award in 2015 and Education Award in 2017 from the IEEE Communications Society (ComSoc), and Technical Recognition Award from Wireless Communications Technical Committee (2019) and AHSN Technical Committee (2013). He has also received the Excellent Graduate Supervision Award in 2006 from the University of Waterloo and the Premier's Research Excellence Award (PREA) in 2003 from the Province of Ontario, Canada. He is the Past President of the IEEE Communications Society. He was the Vice President for Technical & Educational Activities, Vice President for Publications, Member-at-Large on the Board of Governors, Chair of the Distinguished Lecturer Selection Committee, and Member of IEEE Fellow Selection Committee of the ComSoc. Dr. Shen served as the editor-in-chief of the *IEEE IoT Journal*, *IEEE Network*, and *IET Communications*.